

# NITROUS OXIDE (N<sub>2</sub>O) in MACQUARIE HARBOUR, TASMANIA

Maxey, Johnathan Daniel<sup>1,2</sup>, Neil D. Hartstein<sup>2</sup>, Hermann W. Bange<sup>3</sup>, Moritz Müller<sup>1</sup>

<sup>1</sup>Faculty of Engineering, Computing and Science, Swinburne University of Technology, Kuching 93350, Malaysia

<sup>2</sup>ADS Environmental Services, Kota Kinabalu, Sabah, 88400, Malaysia

<sup>3</sup>GEOMAR Helmholtz Centre for Ocean Research Kiel, Wischhofstr. 1-3, 24148 Kiel, Germany

*Correspondence to:* Johnathan Daniel Maxey, Neil D. Hartstein, Hermann W. Bange, and Moritz Müller

## Abstract.

Fjord-like estuaries are hotspots of biogeochemical cycling due to steep physicochemical gradients. The spatiotemporal distribution of nitrous oxide (N<sub>2</sub>O) within many of these systems is poorly described, especially in the southern hemisphere. The goal of this study is to describe the spatiotemporal distribution of N<sub>2</sub>O within a southern hemisphere fjord-like estuary, describe the main environmental drivers of this distribution, the air/sea flux of N<sub>2</sub>O, and the main drivers of N<sub>2</sub>O production. Sampling surveys were undertaken in Macquarie Harbour, Tasmania to capture N<sub>2</sub>O concentrations and water column physicochemical profiles in winter (July 2022), spring (October 2022), summer (February 2023), and autumn (April 2023). N<sub>2</sub>O samples were collected at one depth at system end members, and at 5 depths at 4 stations within the harbour.

Results indicate that N<sub>2</sub>O is consistently supersaturated (reaching 170% saturation) below the system's freshwater lens where oxygen concentrations are often hypoxic, but infrequently anoxic. In the surface lens, levels of N<sub>2</sub>O saturation vary with estimated river flow and with proximity to the system's main freshwater endmember. The linear relationship between apparent oxygen utilization and  $\Delta$ N<sub>2</sub>O saturation indicates that nitrification is the process generating N<sub>2</sub>O in the system. When river flow was high (July and October 2022), surface water N<sub>2</sub>O was undersaturated (as low as 70%) throughout most of the harbour.

When river flow was low (February and April 2023) N<sub>2</sub>O was observed to be supersaturated at most stations. Calculated air/sea fluxes of N<sub>2</sub>O indicated that the system is generally a source of N<sub>2</sub>O to the atmosphere under weak river flow conditions and a sink during strong river flow conditions. The diapycnal flux was a minor contributor to surface water N<sub>2</sub>O concentrations, and subhalocline N<sub>2</sub>O is intercepted by the riverine surface lens and transported out of the system to the ocean during strong river flow conditions. In a changing climate, Western Tasmania is expected to receive higher winter rainfall and lower summer rainfall which may augment the source and sink dynamics of this system by enhancing the summer / autumn efflux of N<sub>2</sub>O to the atmosphere.

This study is the first to report observations of N<sub>2</sub>O distribution, generation processes, and estimated diapycnal / surface N<sub>2</sub>O fluxes from this system.

35 **1. Introduction**

Despite the fact that fjords and fjord-like estuaries represent only a small portion of the coastal area worldwide, they are responsible for sequestering 11% of the global organic carbon (C) burial along terrestrial margins (Smith *et al.*, 2015; Bianchi *et al.*, 2018, 2020). These systems are significant sources of greenhouse gasses (GHG) to the atmosphere (Wilson *et al.*, 2020; Rosentreter *et al.*, 2023; Bange *et al.*, 2024). Many are heavily stratified with strong water column physicochemical gradients (Acuña-González *et al.*, 2006; Inall and Gillibrand, 2010; Hartstein *et al.* 2019; Salamena *et al.*, 2021, 2022; Maxey *et al.* 2022). These gradients can be influenced by mesoscale climate drivers like North Atlantic Oscillation (NAO) and Southern Annular Mode SAM (see Austin and Inall 2002; Gillibrand *et al.*, 2005; Maxey *et al.*, 2022) and local scale drivers like fresh water input and marine intrusions (Inall and Gillibrand 2010; Hartstein *et al.*, 2019; Maxey *et al.*, 2020; Salamena *et al.*, 2022).

Nitrous oxide (N<sub>2</sub>O) is a potent greenhouse gas (GHG) whose increased presence in the atmosphere is primarily driven by emissions from agricultural soils (Tian *et al.*, 2020, 2023). With a global warming potential nearly 300 times that of CO<sub>2</sub>, N<sub>2</sub>O is a key focus of climate studies (Myhre *et al.*, 2013; Etminan *et al.*, 2016; Eyring *et al.*, 2021; Forster *et al.*, 2021). Biological N<sub>2</sub>O production occurs through the microbially mediated processes of ammonia oxidation, nitrite (NO<sub>2</sub><sup>-</sup>) reduction, and nitrate (NO<sub>3</sub><sup>-</sup>) reduction (Kuypers *et al.*, 2018). In marine systems N<sub>2</sub>O production is influenced by environmental conditions such as dissolved oxygen (DO) availability, inorganic nitrogen (N) availability, light availability, temperature (*e.g.* Raes *et al.*, 2016), pH (*e.g.* Breider *et al.*, 2019), and microbial community composition (*e.g.* Wu *et al.* 2020). Many coastal systems are experiencing a reduction in DO availability (Limburg *et al.*, 2020; Testa *et al.*, 2023) and an increased presence of N<sub>2</sub>O as a consequence (Laffoley and Baxter 2019; Ji *et al.*, 2020; Wilson *et al.*, 2020; Wan *et al.*, 2022; Orif *et al.*, 2023; Resplandy *et al.*, 2024).

Estuarine systems often have disproportionately high biological productivity relative to other marine systems (Walinsky *et al.*, 2009; Gilbert *et al.*, 2010; Bianchi *et al.*, 2018, 2020). This also applies to N<sub>2</sub>O dynamics with approx. 33% of marine N<sub>2</sub>O emissions coming from estuaries (Bange *et al.*, 1996; Seitzinger *et al.*, 2000; Murry *et al.*, 2015; Reading, 2022; Rosentreter *et al.*, 2023). Estuaries can act as net sinks (Maher *et al.*, 2016; Wells *et al.*, 2018) or sources (De Bie *et al.*, 2002; Zhang *et al.*, 2010; Sánchez-Rodríguez *et al.*, 2022) of N<sub>2</sub>O depending on physical drivers of air/sea fluxes including waterbody/atmospheric concentration gradients, current velocities, depth, and wind speed (Wells *et al.*, 2018; Bange *et al.* 2019). Other factors include land use modification (Reading *et al.*, 2020; Chen *et al.*, 2022) and the presence of microplastics (Chen *et al.*, 2022). Despite the advancements made thus far, our understanding of marine N<sub>2</sub>O distribution and atmospheric emissions is poorly constrained and needs improvement (Bange *et al.*, 2019, 2024), especially in southern hemisphere fjord-like systems (Yevenes *et al.*, 2017). Much of the current uncertainty lies with a lack of in-situ data describing seasonal N<sub>2</sub>O dynamics to constrain global emissions models (Bange *et al.*, 2019).

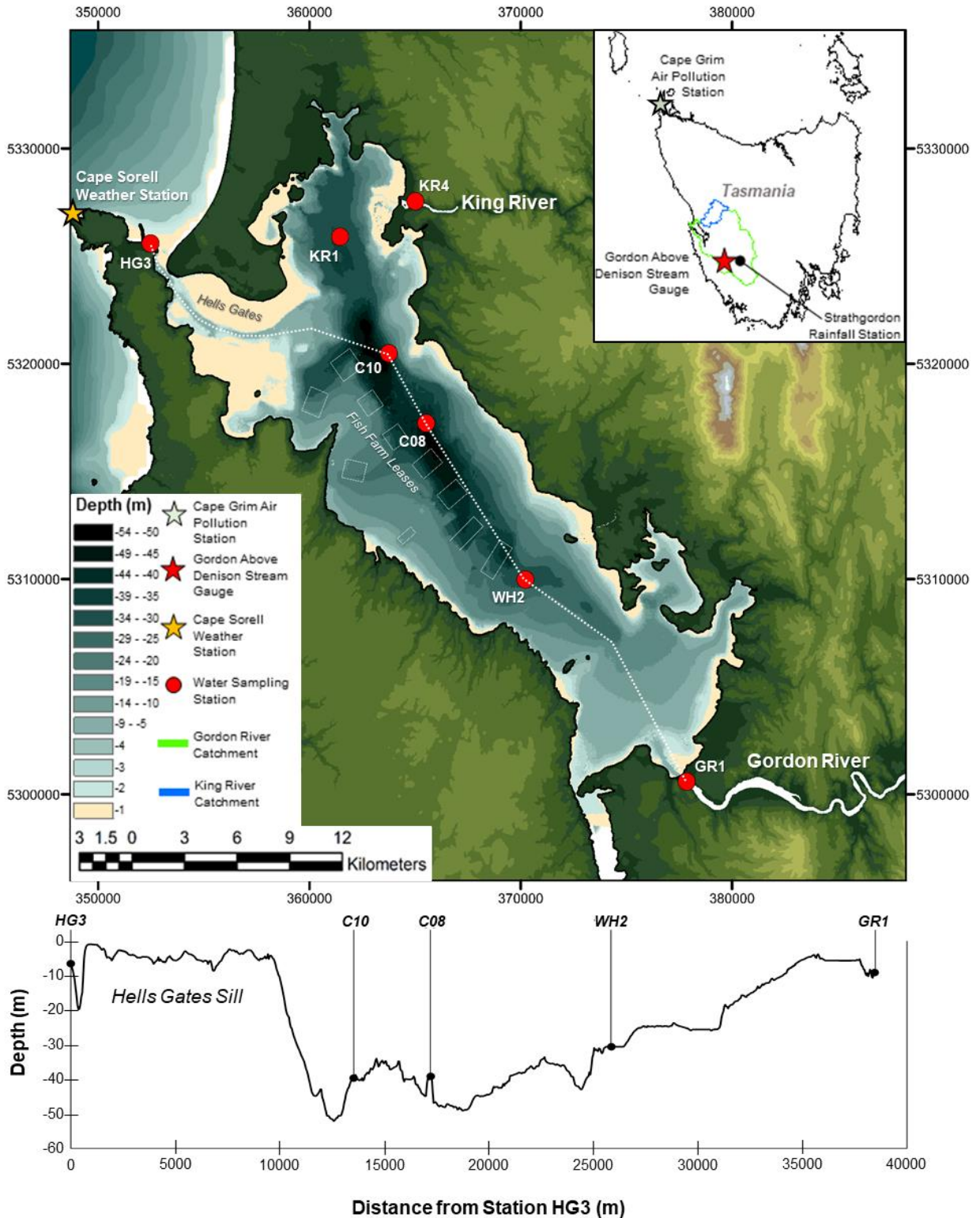
The purpose of this study was (1) to investigate the distribution and seasonal variability of N<sub>2</sub>O concentrations and emissions in a southern hemisphere fjord-like estuary and (2) to decipher the major physical and biological drivers of these emissions.

## 2. Methods

### 2.1 Study Area

75 Macquarie Harbour is a southern hemisphere fjord-like estuary located on Tasmania, Australia's west coast  
(**Figure 1**). The harbour is oriented NW by SE, and is approximately 33 km long, 9 km wide, with a surface area  
of 276 km<sup>2</sup>. The mouth of the harbour is constricted by a shallow (4-8m), long (14km) sill known as "Hells  
Gates". Hells Gates muffles tidal forcing resulting in harbour water levels primarily determined by river flow  
and wind set up (**Hartstein et al., 2019**). The morphology of this system results in sharp gradients of DO,  
80 salinity, and temperature which are seasonally dependant (**Creswell et al., 1989; Hartstein et al., 2019; Maxey  
et al., 2022**). In surface waters dissolved oxygen (DO) concentrations are nearly always in equilibrium with the  
air but decrease sharply through the halocline (~8m to 15m). There is almost no DO produced below the  
halocline (8m to 12m deep) due to high chromophoric dissolved organic matter (CDOM) levels limiting primary  
production at the surface (**Maxey et al., 2017, 2020**). Subhalocline layers (~15m to a few meters from the  
85 bottom) are observed to have DO concentrations below 62.5  $\mu\text{M}$  more than 50% of the time (*see* **Maxey et al.,  
2022**). Near the seabed, episodic marine intrusions (deep water renewal) refresh the supply of DO near the  
mouth of the system but refresh the upper reaches of the harbour less frequently (*see* **Andrewartha and Wild-  
Allen 2017; Hartstein et al., 2019; Maxey et al., 2022**). This process is driven by low atmospheric pressure,  
sustained NW winds, and low catchment rainfall which itself is influenced by Southern Annular Mode (SAM)  
90 (**Hartstein et al., 2019; Maxey et al., 2022**). In the harbour's upper reaches DO concentrations fall below 31  
 $\mu\text{M}$  nearly a third of the time (**Maxey et al., 2022**). Hydrodynamic and oxygen tracer numerical model  
simulations of the harbour by **Andrewartha and Wild-Allen (2017)** estimate that 50% of the harbour's basin  
waters are replaced every 65 days during low river flow conditions and approximately 110 days during normal  
flow conditions.

95 The main source of freshwater to the harbour is located on its southeast end (the Gordon River) and  
drains a nearly pristine catchment (including the Franklin River) of approximately 5,682 km<sup>2</sup> (**Macquarie  
Harbour Dissolved Oxygen Working Group, 2014; Fig 1**). The Gordon River discharges an estimated  
180,000 tons organic carbon (OC) per year into the estuary (**Maxey et al., 2020, 2022**). It should be noted that  
this area receives the some of the highest rainfall (more than 2,500 mm year<sup>-1</sup>) volume in Australia (**Dey et al.,  
100 2019**). The King River, located on the harbour's northern end, is the second largest contributor of fresh water to  
the estuary and drains a catchment area of 802 km<sup>2</sup>. Unlike the Gordon River, the King River has a history of  
receiving treated mining (*e.g.* copper) effluent and transporting this to the harbour (**Carpenter et al., 1991;  
Teasdale et al., 2003**).



105 **Figure 1: Macquarie Harbour, Tasmania. Water sampling stations shown with red circles; Cape Grim Air Pollution**  
**monitoring station shown as a green star (see inset map). Cape Sorell Weather Station shown as an orange star.**  
**Gordon Above Denison stream gauge shown as a red star (see inset map). Aquaculture lease boundaries are shown as**  
**hollow rectangles. Lease locations are sourced from Land Information Systems Tasmania (LISTmap -**  
<https://maps.thelist.tas.gov.au/>**).** Station names reflect general harbour locations where KR1 indicates King River 1;  
 110 C10 and C08 indicate Central Harbour 10 and 08 respectively; WH2 indicates World Heritage Area 2; and GR1  
 indicates Gordon River station 1. Coordinates are displayed in GDA\_1994\_MGA\_Zone\_55. Bathymetry through the  
 system shown as a dashed line, note that this track excludes stations KR4 and KR1.

## 2.2 Experimental Design

115 Nitrous oxide distribution was assessed by collecting water samples across 7 stations, including the  
harbour's endmembers (mouths of the Gordon and King Rivers as well as the harbour mouth at Hells Gates  
Inlet; *see* **Figure 1** and **Table 1**) and stations along the longitudinal axis of the harbour where the deepest basins  
are located (named KR1, C10, C08, and WH2). Samples collected at endmember stations were collected from a  
single depth as these stations are shallow. Samples in the harbour body were collected at 5 depths from the  
120 surface (2m) to approx. 1m from the seabed. Collection campaigns were conducted in July 2022, October 2022,  
February 2023, and April 2023. At each station and depth, three replicate vials ( $n = 3$ ) were collected for the  
determination of  $N_2O$  concentration.

## 2.3 Field Sampling

125 At each station, water quality sonde profiles were collected from the surface to the seabed at 1 meter  
intervals using a YSI EXO-1 equipped with optical DO (accuracy from 0 to 625  $\mu M \pm 3 \mu M$  or 1% of reading  
whichever is greater; precision is 0.03  $\mu M$ ), salinity (accuracy  $\pm 0.1$  or 1% of reading whichever is greater;  
precision is 0.01), temperature (accuracy is  $\pm 0.15$   $^{\circ}C$ ; precision is 0.01  $^{\circ}C$ ), and depth sensors. Sonde calibration  
was checked and corrected (when needed) each sampling period.

130 Water samples were collected at various depths (*see* **Table 1**) using a 5 L Niskin bottle sampler. Water  
sample parameters include dissolved Total Ammoniacal N ( $NH_3 + NH_4^+$ ) (TAN),  $NO_3^-$ , and  $N_2O$ .  $N_2O$  samples  
were collected in triplicate immediately after retrieval of the Niskin bottle by transferring water from the bottle  
through silicone tubing into a 20 mL borosilicate vial. Sample water was added to the vial by placing the tubing  
at the bottom and allowing the vial to overflow several volumes before sealing with a butyl rubber stopper and  
135 aluminium crimp. After ensuring the sample vial was bubble free, 50  $\mu L$  of saturated mercury chloride ( $HgCl_2$ )  
solution was injected into the sample to arrest biological activity. All  $N_2O$  samples were shipped to GEOMAR in  
Kiel, Germany for analysis. Samples were measured in July/August 2023 within 4 to 12 months after sampling  
and were not affected by the storage time (**Wilson et al., 2018**).

140 Water collected for dissolved inorganic N was filtered immediately using 0.45  $\mu m$  polyethersulfone syringe  
filters (Whatman Puradisc). Samples were stored in a chilled dark container until being transported to Analytical  
Services Tasmania in Hobart, Australia for analysis. Dissolved Total TAN and  $NO_3^-$  were analysed using a  
Lachat Flow Injection Analyser. TAN and  $NO_3^-$  analyses used methods based on APHA Standard methods  
(2005) 4500-NH<sub>3</sub> H (reporting limit 0.005  $mg L^{-1}$ ) and 4500 -  $NO_3^- L^{-1}$  (reporting limit 0.002  $mg L^{-1}$ ).

145 **Table 1: Sampling stations showing coordinates, parameters, and sampling depth (in meters).**

Station	Station Depth (m) (MSL)	Dissolved Oxygen Salinity Temperature	$N_2O$	TAN ( $NH_3 + NH_4^+$ )	$NO_3^-$
<b>HG3</b> 352484, 5325594	8	Every Meter	5m	5m	5m
<b>KR4</b> 365018, 5327550	3	1m	1m	1m	1m
<b>KR1</b> 361316, 5325972	36	Every Meter	2, 12, 20, 30, 35m	2, 12, 20, 30, 35m	2, 12, 20, 30, 35m

<b>C10</b> 363708, 5320464	44	Every Meter	2, 12, 20, 30, 42m	2, 12, 20, 30, 42m	2, 12, 20, 30, 42m
<b>C08</b> 365489, 5317238	47	Every Meter	2, 15, 25, 35, 45m	2, 15, 25, 35, 45m	2, 15, 25, 35, 45m
<b>WH2</b> 370218, 5309894	32	Every Meter	2, 12, 20, 25, 30m	2, 12, 20, 25, 30m	2, 12, 20, 25, 30m
<b>GR1</b> 377784, 5300603	12	Every Meter	10m	10m	10m

## 2.4 Analysis of Rainfall and River Loading Estimation

Rainfall and river discharge were analysed using methods presented in **Maxey et al. (2022)** where rainfall and stream gauge data were collected from the Gordon River catchment, Strathgordon rainfall gauge station and the Gordon Above Denison (GAD) stream gauge (**Figure 1**). The rainfall and flow metrics computed include the average daily rainfall over a 20-day period prior to sampling; total accumulated rainfall 20, 10, 5, and 3 days prior to sampling; estimated Gordon River flow into the estuary; and measured flow at the GAD stream gauge.

Gordon River flow was estimated by scaling daily rainfall to the size of the catchment and assuming a rainfall and runoff coefficient of 0.70 adopted from a neighbouring catchment with similar land cover, geology, and slope (**Willis, 2008**). Additional streamflow from Gordon River dam releases was estimated by subtracting scaled rainfall contributions to river flow measured at the GAD stream gauge. This flow was added to the estimated runoff entering the harbour. Rainfall and flow data were provided by the Australian Bureau of Meteorology (BOM).  $\text{NO}_3^-$  and TAN loading was estimated by multiplying the measured concentration of each parameter at station GR1 (*see Figure 1 and Table 1*) by the estimated Gordon River flow.

## 2.5 Analysis of Water Column $\text{N}_2\text{O}$ Concentrations, Air/Sea Flux, and Diapycnal Flux

### 2.5.1 Determination of $\text{N}_2\text{O}$ Concentrations

Water samples were analysed for  $\text{N}_2\text{O}$  using the static-headspace equilibration method followed by gas chromatographic separation (HP Agilent 5890) and detection with an electron capture detector (ECD) as described in **Bange et al. (2019)**, **Bastian (2017)**, and **Kallert (2017)**. The concentration of  $\text{N}_2\text{O}$  in the samples was calculated with the following equation (**Equation 1**; *see Bange et al., 2006*):

**Equation 1**

$$C_{\text{obs}} = \frac{x' PV_{\text{hs}}}{RTPV_{\text{wp}}} + X'\beta P$$

$C_{\text{obs}}$  is the concentration ( $\text{nmol L}^{-1}$ ) of  $\text{N}_2\text{O}$  in the water sample;  $x'$  is the measured dry mole fraction of  $\text{N}_2\text{O}$  in the sample vial's headspace;  $P$  is the ambient pressure set to 1 atm;  $V_{\text{hs}}$  and  $V_{\text{wp}}$  are the volumes of the headspace in the vial and water in the vial;  $R$  is the gas constant;  $T$  is the temperature during equilibrium; and  $\beta$  is the solubility of  $\text{N}_2\text{O}$  (**Weiss and Price, 1980**). The mean relative error of the concentration values obtained was 2.4% ( $\pm 0.16$ ).

### 2.5.2 Estimation of N<sub>2</sub>O Air/Sea Fluxes and N<sub>2</sub>O Saturations

N<sub>2</sub>O air/sea fluxes ( $F$  in  $\mu\text{mol m}^{-2} \text{d}^{-1}$ ) were estimated using equations from **Zhang *et al.*, (2010)** and **Bange *et al.*, (2019)** (Equation 2) Where:

180 Equation 2

$$F = K * (C_{\text{obs}} - C_{\text{eq}})$$

$C_{\text{obs}}$  is the measured concentration ( $\text{nmol L}^{-1}$ ) of N<sub>2</sub>O in the water sample;  $C_{\text{eq}}$  is the air-equilibrated seawater N<sub>2</sub>O concentration, calculated for in situ temperature and salinity using the solubility data of **Weiss and Price (1980)**.  $K$  is the gas transfer velocity, which in the absence of direct measurements can be expressed as a function of the wind speed and the Schmidt Number ( $Sc$ ). For this study we sourced daily average wind speed from the Cape Sorrel Weather Station at the northern end of Macquarie Harbour (<http://www.bom.gov.au/climate/data/index.shtml> station ID 097000; see **Figure 1** for station location).  $K$  was estimated using relationships in **Nightingale (2000)**, **Raymond and Cole (2001)**, and **Wanninkhof (2014)**. Fluxes at Macquarie Harbour's endmember stations used  $K$  values that account for additional forcings like bottom shear (*see* **Raymond and Cole 2001; Zappa *et al.*, 2003; Abril and Borges 2004, Beaulieu *et al.*, 2012; Rosentreter *et al.*, 2021**). Deeper stations in the harbour's main body (*i.e.* KR1, C10, C08, WH2) have surface layers which are separated from the seabed by more than 10 meters. Wind-based  $K_{600}$  estimators were used to estimate air-sea flux in those locations (*see* **Nightingale 2000; Raymond and Cole 2001; Wanninkhof 2014**). Atmospheric N<sub>2</sub>O for this estimation was sourced from monthly mean baseline greenhouse gas mole fractions measured at the Kennaook / Cape Grim Baseline Air Pollution Station, located in north west Tasmania. This station measures atmospheric N<sub>2</sub>O using a gas chromatograph (GC) equipped with an ECD (<https://www.csiro.au/en/research/natural-environment/atmosphere/latest-greenhouse-gas-data>). N<sub>2</sub>O saturation (in %) were computed as  $\text{N}_2\text{O saturation} = 100 * (C_{\text{obs}} / C_{\text{eq}})$ .

### 200 2.5.3 Estimation of Diapycnal N<sub>2</sub>O Flux

N<sub>2</sub>O diapycnal fluxes ( $F_{\text{dia}}$ ; Equation 3) from basin waters (sample depths of 20m or 25m) to the harbour's surface lens (sample depths of 2m) were estimated as:

Equation 3

$$F_{\text{dia}} = K_{\rho} \frac{d[\text{N}_2\text{O}]}{dz}$$

205 Where  $z$  is depth. Diapycnal diffusivity ( $K_{\rho}$ ; Equation 4) was computed with the local buoyancy frequency ( $N^2$ ),  $\Gamma$  set to 0.2 (**Osborn 1980**), and  $\epsilon$  the dissipation rate of turbulent kinetic energy assumed to be on the upper end of values for the mixing zone of stratified systems  $1 \times 10^{-5}$  (**Arneborg *et al.*, 2004; Mickett *et al.*, 2004; Fer *et al.*, 2006**).

Equation 4

$$210 K_{\rho} = \Gamma \frac{\epsilon}{N^2}$$

## 2.6 Data Analysis

The relationships between N<sub>2</sub>O saturation and water quality parameters such as DO concentration, salinity, temperature, nitrate, and ammonium concentrations determined using Pearson correlation. Differences in mean N<sub>2</sub>O saturation between season, depth and each sampling station were tested using a 2-way ANOVA. Differences between rainfall / river flow metrics between seasons were tested using 1-way ANOVA and where significant differences between seasons were detected pair-wise testing using Bonferroni's correction was undertaken. The relationship between rainfall / river flow metrics, from the Gordon River, and surface water N<sub>2</sub>O saturation / N<sub>2</sub>O air/sea flux, at each station, was analysed using Pearson correlation. Standard deviation (std. dev.) of the mean air/sea flux and diapycnal flux was computed from error propagated from replicate observations of N<sub>2</sub>O wind speed, N<sub>2</sub>O concentration, and density (where appropriate) using methods from **Ku (1966)**. Contour plots were made with Plotly Chart Studio: Plotly Technologies Inc. Title: Collaborative data science Publisher: Plotly Technologies Inc. Place of publication: Montréal, QC Date of publication: 2015 URL: <https://plot.ly>



## 225 3. Results

### 3.1 Rainfall and River Loading

Twenty-day rainfall accumulation ranged from a low of 117 mm in July 2022 to a high of 139 mm in April 2023 (see **Figure 2a**). Average ( $\pm$  se) daily rainfall was similar across all months and ranged from 5.12 ( $\pm$  2.57) mm in July 2022 to 5.79 ( $\pm$  3.03) mm in October 2022 (see **Figure 2b**) with no seasonal differences detected ( $p = 0.4326$ ).

Estimated flow at the Gordon River mouth and GAD stream gauge was greater in July and October 2022 than February and April 2023 (**Figure 2c**). Significant seasonal differences in flow measured at the GAD stream gauge were detected ( $p = 5.5 \times 10^{-7}$ ); with greatest flow in July and October 2022 and decreasing over February and April 2023. July flows at the GAD stream gauge were observed to be 107.6 ( $\pm$  15.9)  $\text{m}^3 \text{s}^{-1}$  and in April 2023 were observed to be 30.5 ( $\pm$  2.2)  $\text{m}^3 \text{s}^{-1}$  (**Figure 2d**).

Estimated  $\text{NO}_3^-$  and TAN loading varied with  $\text{NO}_3^-$  loads of 1.69 tonnes  $\text{day}^{-1}$  observed in July 2022, which then dipped to 0.31 tonnes  $\text{day}^{-1}$  in October 2022 and then increased again to 1.77 and 2.77 tonnes  $\text{day}^{-1}$  in February and April 2023 (**Figure 2e**). TAN loading mirrored this pattern with peaks occurring in October 2022 and February 2023 and lows occurring in July 2022 and April 2023.  $\text{N}_2\text{O}$  loading from the Gordon River was observed to be 0.015 tonnes  $\text{day}^{-1}$  in July 2022, 0.012 tonnes  $\text{day}^{-1}$  in October 2022, 0.015 tonnes  $\text{day}^{-1}$  in February 2023, and 0.016 tonnes  $\text{day}^{-1}$  in April 2023 (**Figure 2f**).

### 3.2 Water Column Physicochemical Profiles

DO profiles at the stations located within the main body of the harbour show a well oxygenated surface layer that rapidly attenuates with depth (**Figure 3A**) through the halocline (**Figure 3B**). There is a prominent riverine surface lens in the main harbour extending to depths of up to 8m depending on sampling period and location within the estuary. Salinity in the surface waters was lower in July and October 2022 (6 to 13) than February and April 2023 (greater than 20). Below the halocline salinity ranged from approx. 28 to 32.

The DO gradient between the surface and subhalocline waters was steeper in October relative to July 2022 with October 2022 DO concentrations approaching single digits (3.1  $\mu\text{M}$ ) at station WH2, nearest the Gordon River mouth (see **Figure 1**). In general, the subhalocline concentrations of DO were lower with proximity to the Gordon River mouth. The temperature of the freshwater surface layer ranged from about 9  $^\circ\text{C}$  to 19  $^\circ\text{C}$ , but showed little variation below the halocline where temperature ranged between 13  $^\circ\text{C}$  to 16  $^\circ\text{C}$  (**Figure 3C**).

Nitrate concentrations in the surface water lens tended to be lower than those observed at subhalocline depths (**Figure 4a**). The greatest  $\text{NO}_3^-$  concentrations were observed 2m above the seabed at station WH2 in July and October 2022 as well as mid basin depths at stations C10 and C08 during those same periods with concentrations reaching 1.77  $\mu\text{mol}$ . TAN concentrations were often observed below detection limits (0.3  $\mu\text{mol}$ ), but were greatest in the surface lens or within the halocline itself when detectable (**Figure 4b**). TAN concentrations at WH2 tended to be found at higher levels through the water column relative to other stations (down to about 20m) reaching 1.53  $\mu\text{mol}$  at 15m in October.

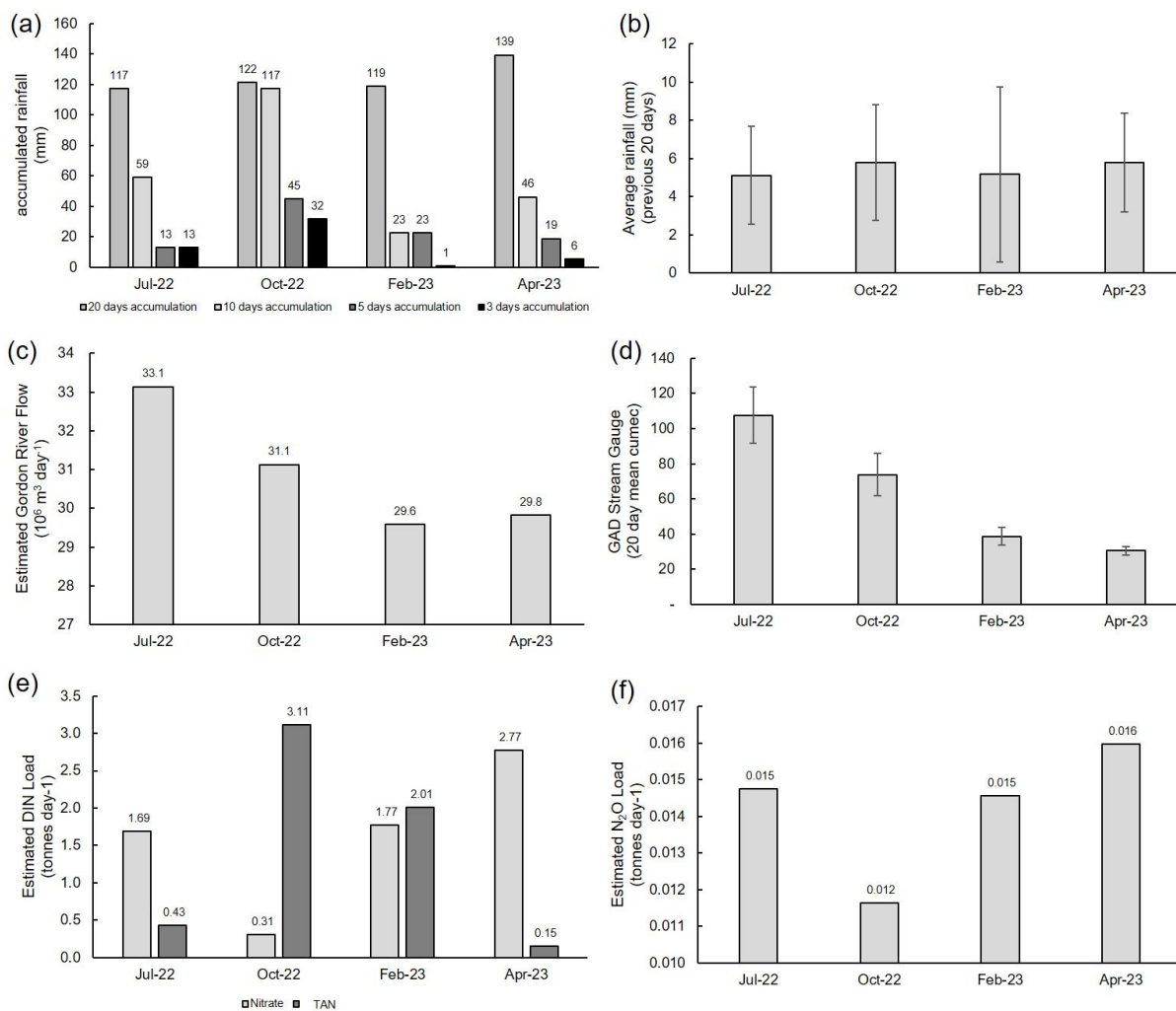
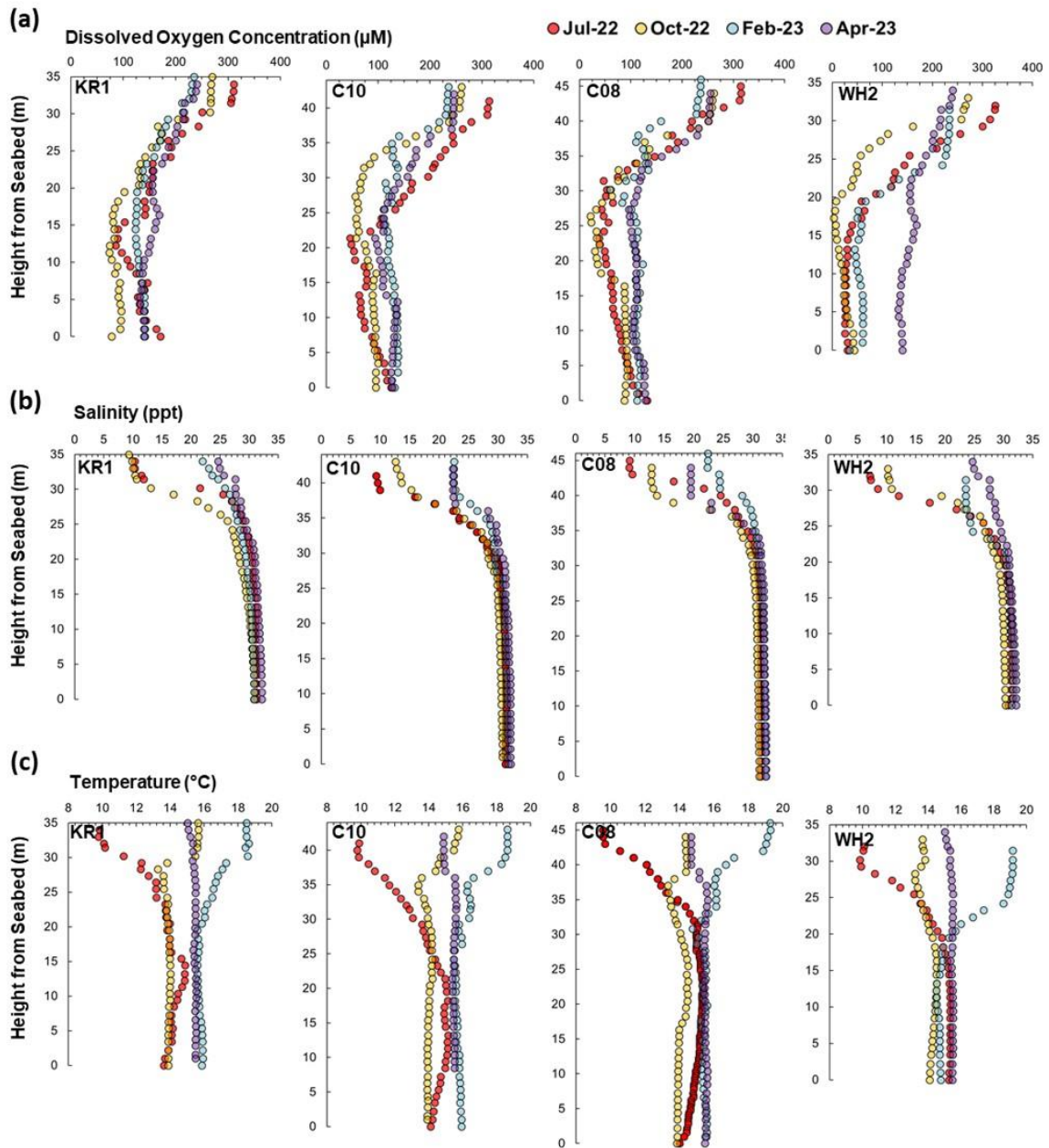
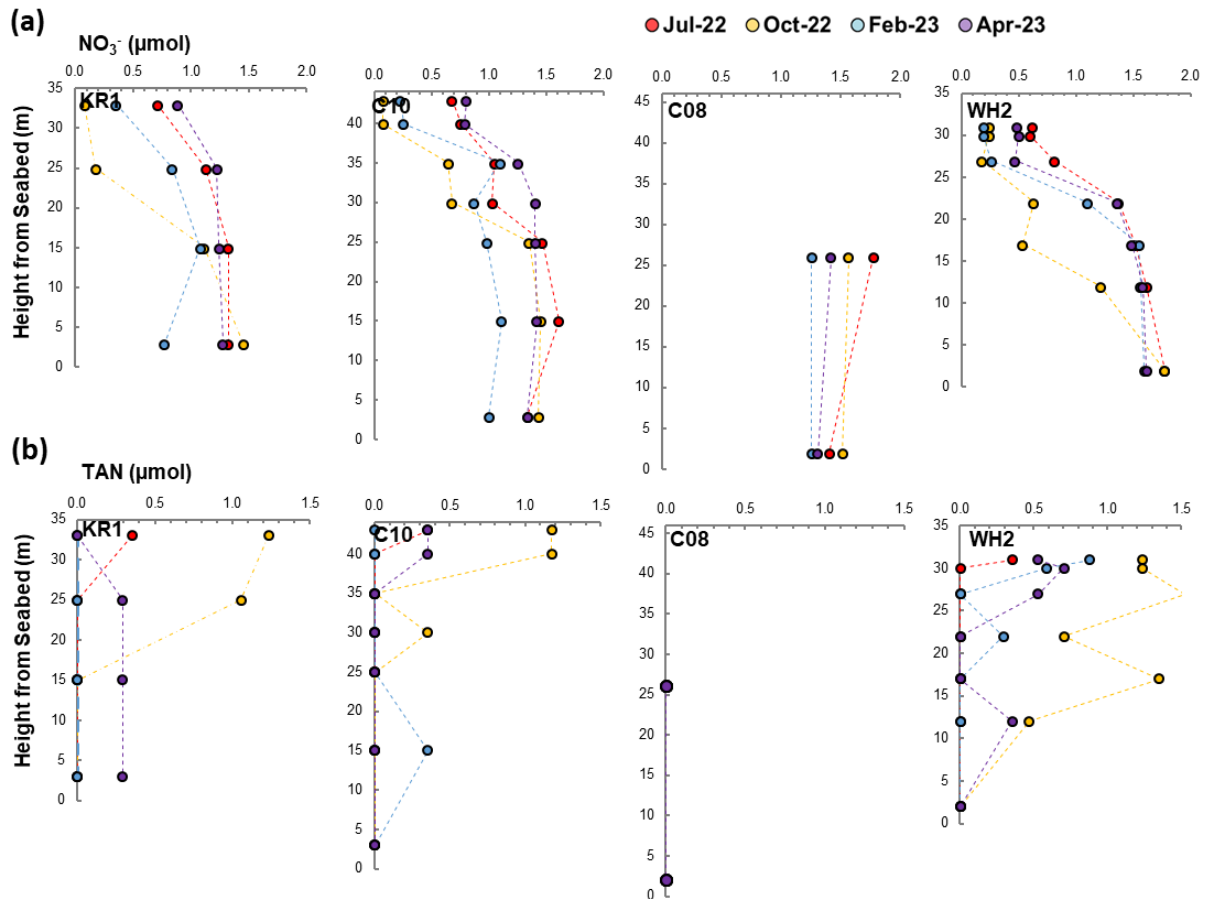


**Figure 2: Rainfall and estimated Gordon River loading estimates for each sampling event. A) accumulated rainfall (mm) 10, 5, and 3 days prior to each sampling event; B) average (mean) daily rainfall over a 20 day period prior to each sampling event; C) estimated Gordon River Flow into the harbour in millions of  $\text{m}^3 \text{ day}^{-1}$ ; D) daily mean flow ( $\text{m}^3 \text{ sec}^{-1}$ ) over previous 20 days prior to sampling ( $\pm$  standard error) at the Gordon Above Denison Stream Gauge; E) estimated nitrate and ammonium loads entering the harbour from the Gordon River; F) estimated  $\text{N}_2\text{O}$  load (tonnes  $\text{day}^{-1}$ ) entering the harbour from the Gordon River.**



270 **Figure 3: Dissolved oxygen ( $\mu\text{M}$ ) (Row A), salinity (Row B), and temperature ( $^{\circ}\text{C}$ ) (Row C) profiles (referencing height from seabed) collected at stations KR1, C10, C08, and WH2 in July 2022 (red dots), October 2022 (yellow dots), February 2023 (blue dots), and April 2023 (purple dots). Measurements were made every 1 meter.**

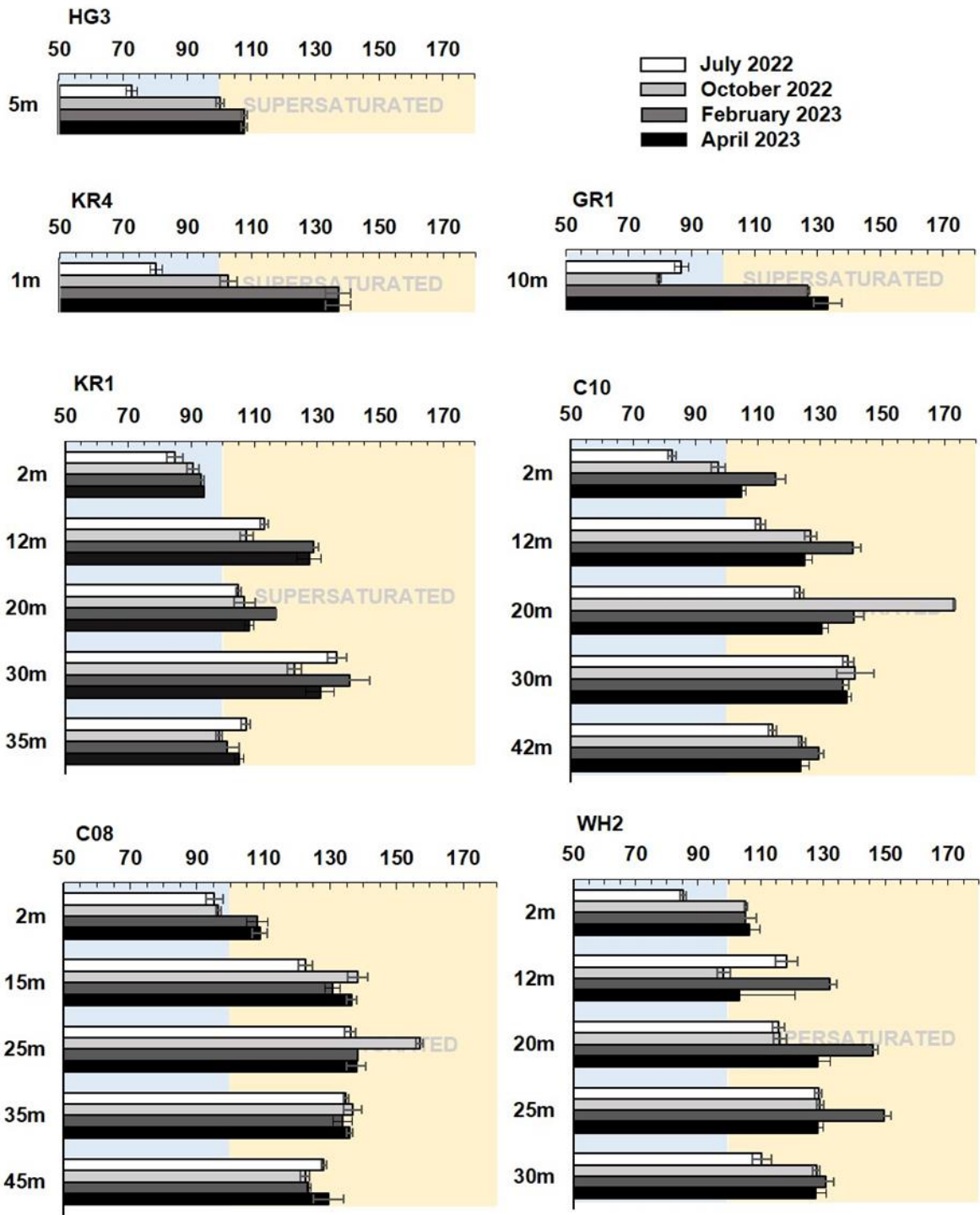


275 **Figure 4:** Nitrate  $\text{NO}_3^-$  (row a) and TAN (row b) concentrations with depth (referencing height from seabed) collected at stations KR1, C10, C08, and WH2 in July 2022 (red dots), October 2022 (yellow dots), February 2023 (blue dots), and April 2023 (purple dots). Data presented as having a concentration of 0.0 are below the detection limits of the analyte.

### 3.3 $\text{N}_2\text{O}$ Distribution

280 At each harbour station, depth and season (and their interaction) significantly impacted  $\text{N}_2\text{O}$  saturation (two-way ANOVA,  $\alpha = 0.05$ , *degree of freedom* (*d.f.*) = 59). At 2 m,  $\text{N}_2\text{O}$  saturation was observed to be below 100% at all stations in July 2022 (**Figure 5** and **Figure 6**) and at stations KR1, C10, and C08 in October 2022. In February and April 2023  $\text{N}_2\text{O}$  saturation in the harbour was above 100% through the water column except in KR1 surface waters. The maximum  $\text{N}_2\text{O}$  concentrations were observed in the subhalocline. Among the subhalocline observations the maximum  $\text{N}_2\text{O}$  concentrations (reaching over 170%) were observed at the base of the Hells Gates sill at station C10 in October 2022.

285 All endmember  $\text{N}_2\text{O}$  concentrations were undersaturated in July 2022. In October, stations KR1 and HG3 were observed to be approx. 100% saturated but  $\text{N}_2\text{O}$  at station GR1 was undersaturated. In February and April 2023  $\text{N}_2\text{O}$  concentrations were supersaturated at all endmember stations. There were statistically significant linear correlations between  $\text{N}_2\text{O}$  saturation and salinity ( $r = 0.494$ ;  $p = 5.5 \times 10^{-7}$ ,  $n = 92$ ), temperature ( $r = 0.391$ ;  $p = 1.2 \times 10^{-4}$ ,  $d.f. = 90$ ), DO concentration ( $r = -0.563$ ;  $p = 5.2 \times 10^{-9}$ ,  $d.f. = 90$ ), and nitrate concentration ( $r = 0.559$ ;  $p = 6.9 \times 10^{-9}$ ,  $d.f. = 90$ ) in the harbour stations (**Figure 7**). The correlation between  $\text{N}_2\text{O}$  saturation and the TAN concentration however was not statistically significant ( $r = 0.174$ ;  $p = 0.31$ ,  $d.f. = 34$ ).



295 **Figure 5:** Mean ( $\pm$  standard error) N<sub>2</sub>O % saturation observed at each sampling station, with depth, and across seasons. Note that a red dashed line indicating 100% at the time of sampling has been placed on each panel for reference.

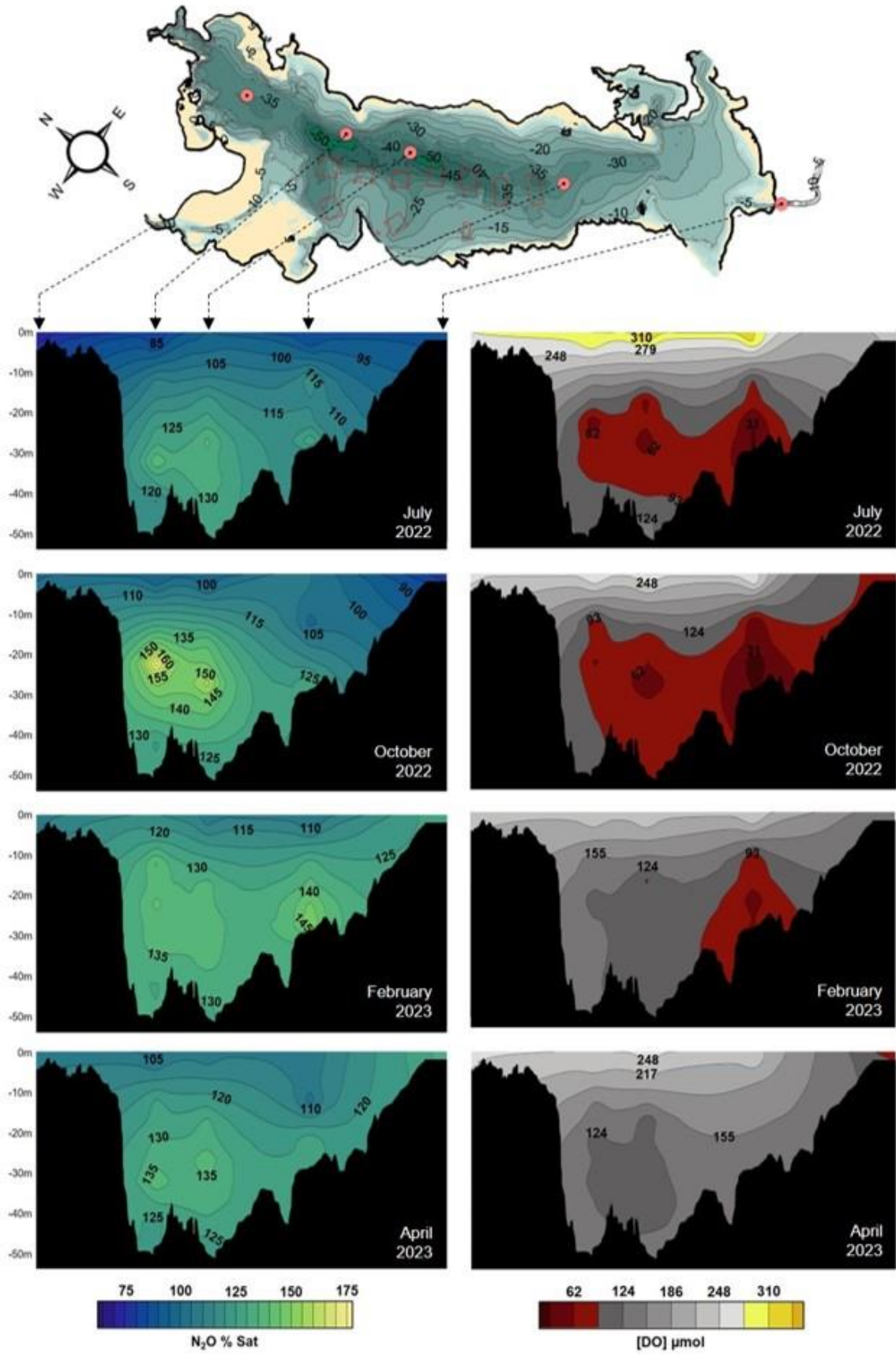
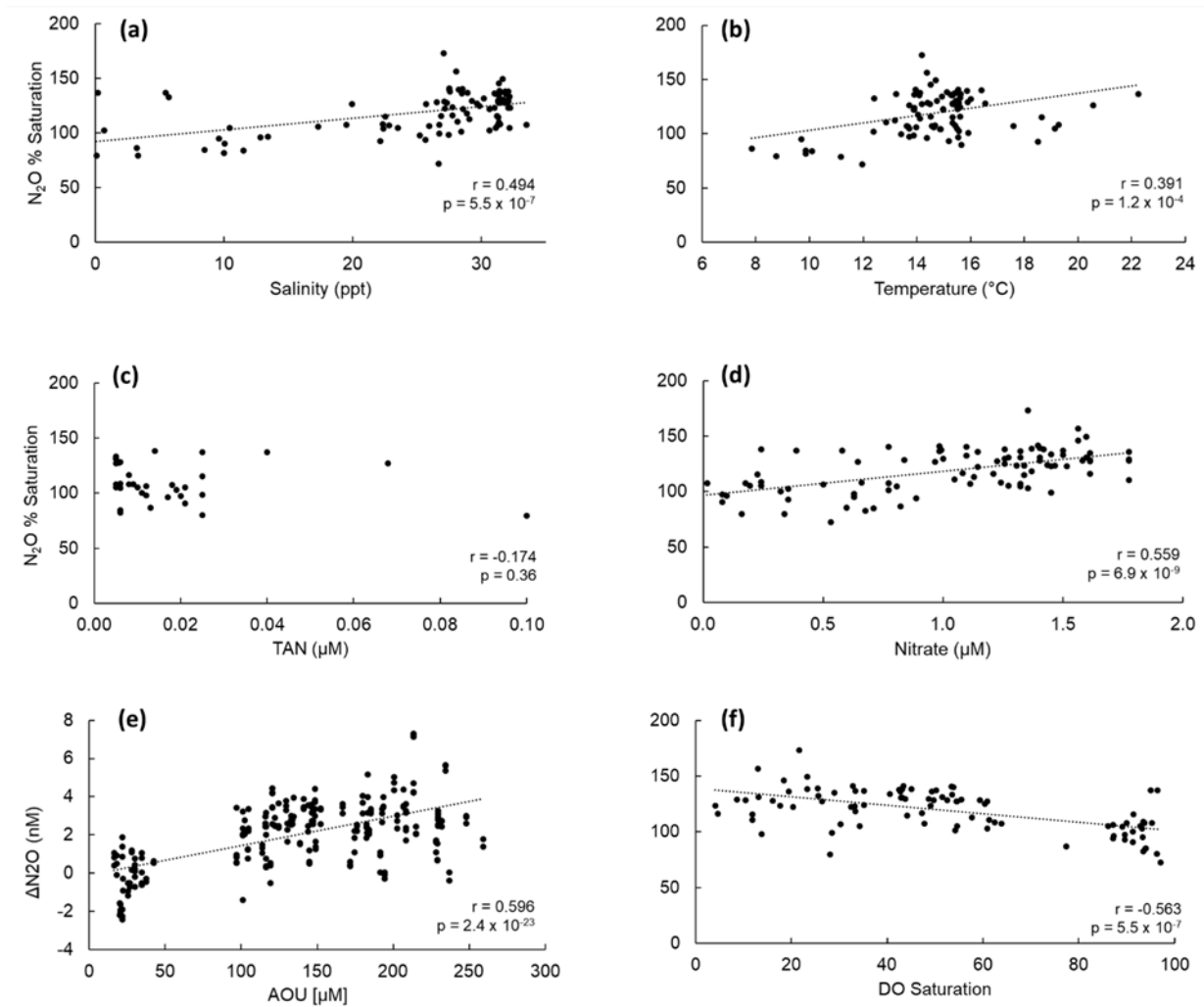


Figure 6: Contour plots of mean N<sub>2</sub>O % saturation (left column) and mean DO concentration in units of μmol (right column) observed at stations HG3, C10, C08, WH2, and GR1 from July 2022 to April 2023. Red shaded areas on the DO plots indicate low oxygen concentrations (< 93 μmol). Relative positions of the stations are shown on the top left panel. Y-axis displays depth in metres relative to mean sea level.

300



305 **Figure 7: Correlation between N<sub>2</sub>O % saturation observed across the harbour and a) Salinity, b) Temperature, c) Total Ammoniacal Nitrogen (TAN) concentration, d) Nitrate concentration. The correlation between AOU [µM] and ΔN<sub>2</sub>O [nM] is shown in panel e). The relationship between N<sub>2</sub>O % saturation and DO % saturation is shown in panel f). Pearson correlation coefficients (r) and their associated p value are shown in each panel.**

### 310 **3.4 N<sub>2</sub>O Air/Sea and Diapycnal Fluxes**

Atmospheric N<sub>2</sub>O mole fractions measured at Kinnaook / Cape Grim Air Pollution Station (*see Figure 1*) were observed to increase from 334.7 ppb in July 2022 to 335.9 ppb in February 2023. The April 2023 atmospheric N<sub>2</sub>O mole fraction was slightly lower than that observed in February 2023 at 335.6 ppb. Average (± std. dev.) wind speeds were observed to be 6.6 (± 3.7) m sec<sup>-1</sup> in July, 5.6 (± 2.5) m sec<sup>-1</sup> in October, 6.3 (± 3.4) m sec<sup>-1</sup> in February, and 6.4 (± 4.0) m sec<sup>-1</sup> in April.

Estimated N<sub>2</sub>O air/sea flux in the main harbour stations (KR1, C10, C08, WH2) ranged from -12.88 (± 6.00) µmol N<sub>2</sub>O m<sup>-2</sup> day<sup>-1</sup> at C10 in July 2022 (negative sign indicates absorption of N<sub>2</sub>O into the surface waters from the atmosphere) to 7.31 (± 3.43) µmol N<sub>2</sub>O m<sup>-2</sup> day<sup>-1</sup> at the same station in February 2023 (using the “High” K<sub>600</sub> estimator from **Raymond and Cole (2001)**; *see Table 2*)

320 Station KR1 was always observed to be a site of atmospheric N<sub>2</sub>O uptake and was every non-endmember station in July 2022. Near the head of the system, station WH2 was observed to be a net source of N<sub>2</sub>O to the

atmosphere from October 2022 to April 2023, and stations C10 and C08 (positioned above the deepest basins) were net sources in February 2023 and April 2023.

325 Estimated diapycnal fluxes ( $\pm$  std. dev.) using local buoyancy frequencies showed a consistent upwards movement of  $\text{N}_2\text{O}$  from the subhalocline to surface layers with the smallest fluxes observed in July 2022 ( $49 \pm 2.3 \text{ nmol N}_2\text{O m}^{-2} \text{ day}^{-1}$  at C08) and largest fluxes observed in October 2022 (up to  $1308 \text{ nmol N}_2\text{O m}^{-2} \text{ day}^{-1}$  at WH2) and February 2023 (up to  $1200 \pm 47.3 \text{ nmol N}_2\text{O m}^{-2} \text{ day}^{-1}$  at C10) see Error! Reference source not found.. Patterns in the size of the diapycnal flux generally reflected the patterns of  $\text{N}_2\text{O}$  % saturation with the largest fluxes occurring in October 2022 during the periods of greatest  $\text{N}_2\text{O}$  % saturation. Overall the magnitude  
330 of the estimated diapycnal fluxes was smaller than estimated air/sea fluxes.

332



333 **Table 2: Estimated sea-to-air N<sub>2</sub>O flux (mean  $\mu\text{mol N}_2\text{O m}^{-2} \text{ day}^{-1} \pm \text{std. dev.}$ ) of the main harbour stations using**  
 334 **calculations presented in Bange et al. (2019) and Zhang et al. (2020) and a range of  $k_{600}$  parameterisations from**  
 335 **Wanninkhof (2014;  $W_{2014}$ ), Raymond and Cole (2001;  $RC_{\text{Low}}$ ,  $RC_{\text{Mid}}$ , and  $RC_{\text{High}}$ ), and Nightingale (2000;  $N_{2000}$ ).**  
 336 **Positive values indicate the flux of N<sub>2</sub>O from the harbour water to the atmosphere. Negative values (shown in with**  
 337 **bold text) indicate flux of N<sub>2</sub>O from the atmosphere into the harbour water. Estimated Gordon River Flow and Mean**  
 338 **(20 day) Gordon Above Dennison (GAD)Stream Gauge are also shown for each month as well as the Pearson**  
 339 **Correlation and associated p-values between flow metrics, rainfall, and air/sea flux (and surface water % saturation).**

Station	$K_{600}$	Jul 2022 $\mu\text{mol N}_2\text{O m}^{-2} \text{ day}^{-1}$	Oct 2022 $\mu\text{mol N}_2\text{O m}^{-2} \text{ day}^{-1}$	Feb 2023 $\mu\text{mol N}_2\text{O m}^{-2} \text{ day}^{-1}$	Apr 2023 $\mu\text{mol N}_2\text{O m}^{-2} \text{ day}^{-1}$	Gordon Flow vs Surface Flux	GAD Flow vs Surface Flux	GAD Flow vs % N <sub>2</sub> O Sat.	Rainfall vs Surface Flux
KR1	$RC_{\text{High}}$	<b>-11.07 ± 5.17</b>	<b>-04.01 ± 1.77</b>	<b>-03.30 ± 1.54</b>	<b>-03.17 ± 1.66</b>	$r = -0.8316$ $p = 7.5 \times 10^{-4}$	$r = -0.8624$ $p = 3.1 \times 10^{-4}$	$r = -0.8726$ $p = 2.1 \times 10^{-4}$	$r = 0.5577$ $p = 0.060$
	$RC_{\text{Mid}}$	<b>-08.45 ± 4.42</b>	<b>-03.19 ± 1.59</b>	<b>-02.55 ± 1.34</b>	<b>-02.44 ± 1.41</b>				
	$RC_{\text{Low}}$	<b>-04.69 ± 3.17</b>	<b>-01.93 ± 1.27</b>	<b>-01.46 ± 0.99</b>	<b>-01.38 ± 0.99</b>				
	$N_{2000}$	<b>-0.85 ± 0.31</b>	<b>-0.30 ± 0.08</b>	<b>-0.25 ± 0.09</b>	<b>-0.24 ± 0.11</b>				
	$W_{2014}$	<b>-0.78 ± 0.25</b>	<b>-0.27 ± 0.05</b>	<b>-0.23 ± 0.07</b>	<b>-0.22 ± 0.09</b>				
C10	$RC_{\text{High}}$	<b>-12.88 ± 6.00</b>	<b>-01.21 ± 0.53</b>	07.31 ± 3.43	02.60 ± 1.36	$r = -0.8298$ $p = 8.4 \times 10^{-4}$	$r = -0.9091$ $p = 4.2 \times 10^{-5}$	$r = -0.8795$ $p = 1.6 \times 10^{-4}$	$r = 0.2751$ $p = 0.387$
	$RC_{\text{Mid}}$	<b>-09.83 ± 5.14</b>	<b>-00.96 ± 0.48</b>	05.65 ± 2.98	02.00 ± 1.16				
	$RC_{\text{Low}}$	<b>-05.46 ± 3.68</b>	<b>-00.58 ± 0.38</b>	03.22 ± 2.19	01.13 ± 0.81				
	$N_{2000}$	<b>-0.99 ± 0.36</b>	<b>-0.09 ± 0.02</b>	0.67 ± 0.23	0.20 ± 0.09				
	$W_{2014}$	<b>-0.91 ± 0.29</b>	<b>-0.08 ± 0.02</b>	0.61 ± 0.18	0.18 ± 0.07				
C08	$RC_{\text{High}}$	<b>-03.50 ± 1.63</b>	<b>-01.69 ± 0.74</b>	04.08 ± 1.91	04.57 ± 2.40	$r = -0.8547$ $p = 3.97 \times 10^{-4}$	$r = -0.8804$ $p = 1.6 \times 10^{-4}$	$r = -0.8447$ $p = 5.4 \times 10^{-4}$	$r = 0.1846$ $p = 0.566$
	$RC_{\text{Mid}}$	<b>-02.67 ± 1.40</b>	<b>-01.34 ± 0.67</b>	03.15 ± 1.66	03.52 ± 2.03				
	$RC_{\text{Low}}$	<b>-01.49 ± 1.00</b>	<b>-0.81 ± 0.53</b>	01.80 ± 1.22	01.98 ± 1.43				
	$N_{2000}$	<b>-0.27 ± 0.10</b>	<b>-0.12 ± 0.03</b>	0.31 ± 0.11	0.35 ± 0.15				
	$W_{2014}$	<b>-0.25 ± 0.08</b>	<b>-0.11 ± 0.02</b>	0.29 ± 0.08	0.32 ± 0.13				
WH2	$RC_{\text{High}}$	<b>-10.88 ± 5.06</b>	02.63 ± 1.15	02.40 ± 1.13	03.50 ± 1.84	$r = -0.8071$ $p = 1.51 \times 10^{-3}$	$r = -0.8269$ $p = 9.1 \times 10^{-4}$	$r = -0.8077$ $p = 1.5 \times 10^{-3}$	$r = 0.6316$ $p = 0.028$
	$RC_{\text{Mid}}$	<b>-08.30 ± 4.34</b>	02.09 ± 1.04	01.85 ± 0.98	02.69 ± 1.56				
	$RC_{\text{Low}}$	<b>-04.61 ± 3.11</b>	01.26 ± 0.83	01.06 ± 0.72	01.52 ± 1.09				
	$N_{2000}$	<b>-0.84 ± 0.30</b>	0.19 ± 0.05	0.19 ± 0.06	0.27 ± 0.12				
	$W_{2014}$	<b>-0.77 ± 0.24</b>	0.17 ± 0.03	0.17 ± 0.05	0.25 ± 0.10				
Gordon River Flow ( $\text{m}^3 \text{sec}^{-1}$ )		383.6 ± 38.9	360.3 ± 54.1	342.6 ± 74.6	324.3 ± 26.6	-	-	-	-
GAD Flow ( $\text{m}^3 \text{sec}^{-1}$ )		107.6 ± 15.9	73.7 ± 12.1	38.8 ± 5.1	30.5 ± 2.2	-	-	-	-

340  
341

342 **Table 3: Estimated diapycnal N<sub>2</sub>O flux ( $\text{nmol N}_2\text{O m}^{-2} \text{ day}^{-1} \pm \text{std. dev.}$ ) calculated from local buoyancy frequencies**  
 343 **from 20 m to 2 m within the main harbour stations Positive values indicate the flux of N<sub>2</sub>O from the basin water (20**  
 344 **m) to the surface lens (2m).**

Station	July 2022 $\text{nmol N}_2\text{O m}^{-2} \text{ day}^{-1}$	October 2022 $\text{nmol N}_2\text{O m}^{-2} \text{ day}^{-1}$	February 2023 $\text{nmol N}_2\text{O m}^{-2} \text{ day}^{-1}$	April 2023 $\text{nmol N}_2\text{O m}^{-2} \text{ day}^{-1}$
<b>KR1</b>	80 ± 3.5	282 ± 17.7	992 ± 12.9	395 ± 8.6
<b>C10</b>	140 ± 4.5	1,200 ± 47.3	1,040 ± 65.3	454 ± 16.2
<b>C08</b>	49 ± 2.3	782 ± 12.1	778 ± 37.4	348 ± 18.6
<b>WH2</b>	117 ± 4.0	125 ± 2.8	1,308 ± 67.8	240 ± 18.0

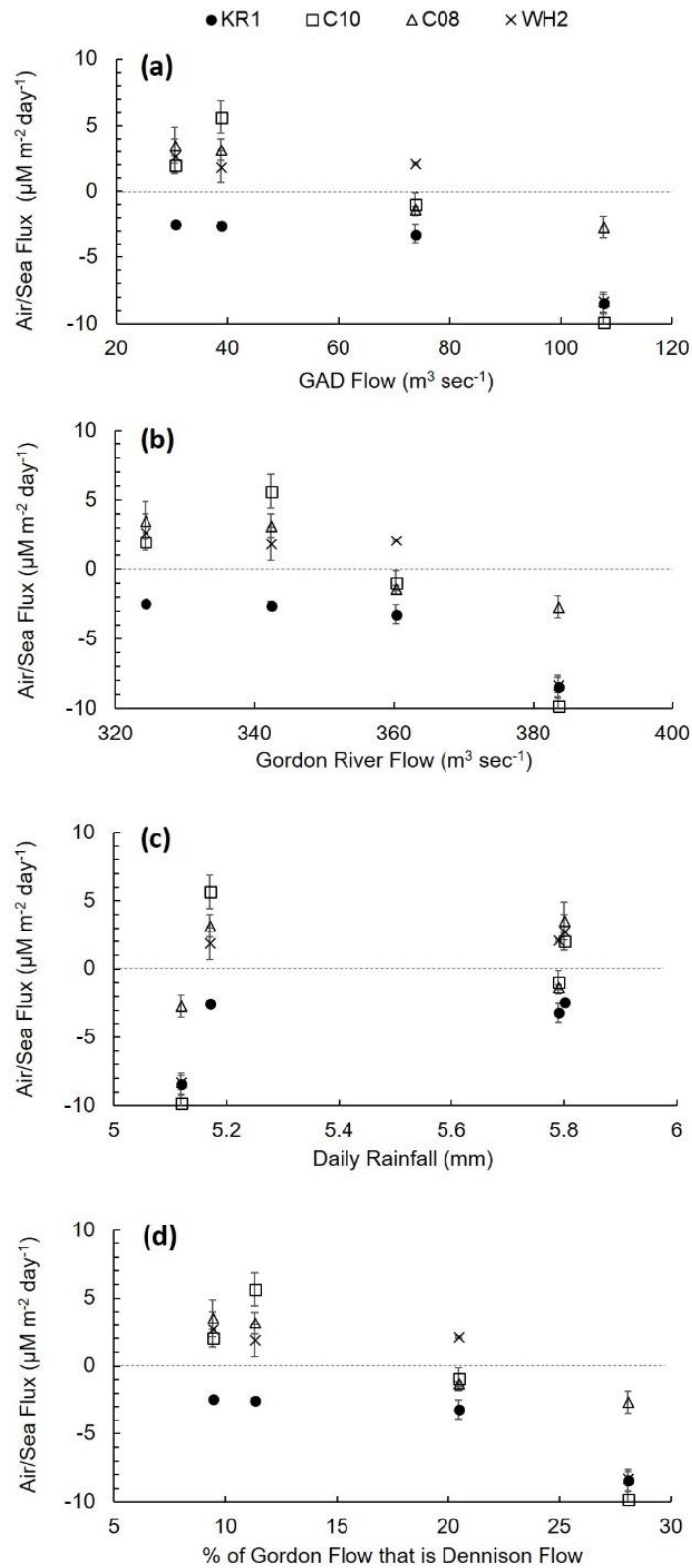
345  
346

#### 347 4. Discussion

348 Our study is the first to report on N<sub>2</sub>O distribution and air/sea flux from an Australasian fjord-like estuary.  
349 We set out to investigate how N<sub>2</sub>O concentrations varied along horizontal and depth gradients; how N<sub>2</sub>O  
350 concentrations and estimated surface water emissions vary seasonally; how N<sub>2</sub>O concentrations vary with  
351 freshwater inputs; and whether the relationship between AOU and  $\Delta$ N<sub>2</sub>O could help clarify the primary  
352 mechanism for N<sub>2</sub>O generation in this system. We used surface water observations, local wind speed (from Cape  
353 Sorell weather station) and atmospheric N<sub>2</sub>O mole fractions (from Cape Grimm; **Figure 1**) to estimate N<sub>2</sub>O  
354 air/sea flux (based on **Zhang et al., 2010** and **Bange et al., 2019**) and found that Macquarie Harbour functions as  
355 both a site of atmospheric uptake and emission of N<sub>2</sub>O. Most harbour stations were estimated to be removing  
356 atmospheric N<sub>2</sub>O in July and October 2022 (when river flow was greater) and emitting N<sub>2</sub>O into the atmosphere  
357 in February and April 2023 (during low river flow periods; *see* **Figure 8** and **Table 2**). Pearson correlations  
358 show that when freshwater flow is high N<sub>2</sub>O air/sea flux is negative (indicating uptake from the atmosphere) and  
359 when freshwater flow is low N<sub>2</sub>O air/sea flux is positive (**Table 2**). Our observations highlight that freshwater  
360 flow is a key driver of N<sub>2</sub>O emissions in this estuary. In addition, Gordon River flow is heavily influenced by  
361 hydroelectric dam release (up to ~28% of the flow in July 2023). Rainfall in the catchment area may offset the  
362 effects of dam release, but our observations did not capture this as rainfall itself was not significantly correlated  
363 with N<sub>2</sub>O concentrations or air/sea flux.

364 The river endmember concentrations of N<sub>2</sub>O were often observed to be undersaturated, as observed in the  
365 South Platte River Basin, USA, **McMahon and Dennehy (1999)**; Neuse River Estuary, USA, **Stow et al.,**  
366 **(2005)**; headwater streams, Ontario, Canada, **Baulch et al., (2011)**; and Upper Mara River Basin, Kenya,  
367 **Mwanke et al., (2019)**. Our observations of endmember N<sub>2</sub>O concentrations were similar to the lower end of the  
368 concentrations reported in **McMahon and Dennehy (1999)** (approx. 80% saturation), but not as low as those  
369 reported Jackson Creek, Ontario, Canada in **Baulch et al., (2011)**, where some observations reached <20%  
370 saturation. N<sub>2</sub>O undersaturation in those systems was attributed to complete denitrification (use of N<sub>2</sub>O as a  
371 terminal electron acceptor by denitrifies) in streams with high DOC loads, low DO, and low NO<sub>3</sub><sup>-</sup>  
372 concentrations. It should also be noted that up to 28% of the estimated Gordon River flow was found to be  
373 associated with flow through the Gordon Above Dennison stream gauge (a proxy for hydroelectric dam/reservoir  
374 release to the Gordon River). Boreal reservoirs have been shown to be net sinks of atmospheric N<sub>2</sub>O (**Hendzel et**  
375 **al., 2005**) which was attributed to increased N<sub>2</sub>O demand to drive complete denitrification. There is good reason  
376 to believe that N<sub>2</sub>O may be scavenged in the Gordon and King Rivers as well because they do often have high  
377 DOC concentrations, high water column DO demand (**Maxey et al., 2020**), and low DO concentrations in near  
378 the stream bed (**Maxey et al., 2022**).

379 Below the estuary's predominately freshwater surface lens, the fjord-like morphology drives suboxic  
380 conditions like those observed in the subhalocline waters at station WH2 in October 2022 (*see* **Figure 3**;  
381 **Hartstein et al., 2019**; **Maxey et al., 2020, 2022**). While these conditions do not always persist, DO  
382 concentrations below 31  $\mu$ M have been observed to occur more than 30% of the time up estuary, specifically at  
383 station WH2 (**Maxey et al., 2022**). In the low DO sub-halocline layers of the harbour we observed the maximum  
384 N<sub>2</sub>O concentrations (**Figure 5** and **Figure 6**). Subhalocline N<sub>2</sub>O saturation was observed to generally range from  
385 approx. 110% to 170% with the highest values observed within the deeper basins near the foot of the sill  
386 (stations C10 and C08; **Figure 6**).



387  
 388 **Figure 8: Mean Air/Sea Flux ( $\mu\text{M m}^{-2} \text{ day}^{-1}$ ) versus a) Gordon above Dennison River flow ( $\text{m}^3 \text{ day}^{-1}$ ), b) estimated**  
 389 **Gordon River flow ( $\text{m}^3 \text{ day}^{-1}$ ), c) daily rainfall (mm) (20 day mean), and d) % of estimated Gordon River flow this is**  
 390 **accounted for by the Gordon above Dennison River gauge (proxy for hydroelectric dam release). Error bars indicate**  
 391  **$\pm 1$  standard error.**

392 In the harbour's subhalocline layer there is not enough light to support photosynthesis (Hartstein *et al.*,  
 393 2019; Maxey *et al.*, 2017, 2020, and 2022) and thus the main source of oxygen is advection from marine  
 394 intrusions.  $\text{N}_2\text{O}$  producing microbes have been observed to populate this layer of the harbour (*see* Da Silva *et al.*,

395 **2021** and **2022**) and our observations of supersaturated N<sub>2</sub>O in these layers show that those microbes are active.  
396 Linear relationships between AOU and ΔN<sub>2</sub>O (slope = 0.0154; r = 0.596; p = 2.4 × 10<sup>-23</sup>; **Figure C**) and NO<sub>3</sub><sup>-</sup>  
397 and N<sub>2</sub>O saturation (r = 0.559; p = 6.9 × 10<sup>-9</sup>; **Figure D**) indicate that N<sub>2</sub>O production likely occurs primarily  
398 through the ammonia oxidation (nitrification) pathway (**Yoshinari, 1976; Walter et al., 2004; Brase et al.,**  
399 **2017**). Our observations are on the lower end of reported N<sub>2</sub>O yield per mole O<sub>2</sub> consumed (see  
400 **Suntharalingam and Sarmiento, 2000; Brase et al., 2017**) which may be an artefact of mixing and loss  
401 dynamics such as basin water DO recharges from marine intrusions, and loss to aerobic respiration and the  
402 atmosphere. This suggests that some portion of subhalocline pelagic oxygen demand in the harbour can be  
403 attributed to nitrifying microbes (albeit at a much lower rate compared to aerobic respiration). **Ji et al., (2020)**  
404 also observed similar relationships in the Saanich Inlet, a seasonally anoxic fjord-like estuary in British  
405 Columbia, but in that system anoxic conditions are more persistent (**Bourbonnais et al., 2013; Manning et al.,**  
406 **2010**) compared to Macquarie Harbour (**Maxey et al., 2022**). Deep-water renewal / marine intrusions have been  
407 hypothesized to stimulate N<sub>2</sub>O production in the Saanich Inlet (**Capelle et al., 2018; Michiles et al., 2019; Ji et**  
408 **al., 2020**), and Baltic Sea (**Walter et al., 2006**) and may also be stimulating it in Macquarie Harbour as well. In  
409 the Baltic Sea, **Walter et al. (2006)** and **Mylykangas et al. (2017)** observed enhanced N<sub>2</sub>O production in areas  
410 receiving significant marine intrusions. Positive correlations between AOU and ΔN<sub>2</sub>O observed in western Baltic  
411 Sea waters (**Walter et al., 2006**) along with mean (11-year; 2006-2017) seasonal variations in DO and N<sub>2</sub>O  
412 observed through the water column at the Boknis Eck Time-Series Station (Eckernförde Bay, Southwest Baltic  
413 Sea) indicate a tight coupling between DO supply and N<sub>2</sub>O production (presumably by nitrification) /  
414 consumption (presumably by denitrification) pathways in that area (**Ma et al., 2019**). The reintroduction of  
415 marine water on the upstream side of a dam in the Nakong River, South Korea was found to affect bottom water  
416 trapping (stagnation), DO conditions, N process rates, process specific gene abundances, and subsequently the  
417 fate of N in that system (**Huang et al., 2024**). Marine intrusions primarily refresh the DO supply adjacent to the  
418 sill in Macquarie Harbour (near station C10). As we observed a positive correlation between AOU and ΔN<sub>2</sub>O  
419 marine intrusions offer a possible explanation for the higher subhalocline N<sub>2</sub>O concentrations observed in this  
420 part of the harbour (*see Error! Reference source not found.*).

421 One other possible pathway of water column N<sub>2</sub>O production might be through denitrification as DO  
422 concentrations at WH2 in October 2022 approached single digits (3.1 μM). This station has the highest basin  
423 residence time compared the others used in this study. Low oxygen concentrations may also likely be found  
424 under the harbour's fish farms due to the aerobic respiration of farm debris (**Maxey et al. 2020**). Though whether  
425 denitrification functions as a production process or a loss process will depend upon the drivers of DO  
426 concentration (*i.e.* respiration rates, physical mixing, *etc.*) and may differ depending on the location of the basins  
427 in this system. It is likely the main driver of undersaturated N<sub>2</sub>O concentrations in the Gordon River.

428 We conceptualize that during periods of high river flow, the surface water lens thickens and transports  
429 water undersaturated with N<sub>2</sub>O quickly across the harbour surface and out of Hells Gates inlet. Some N<sub>2</sub>O from  
430 the continuously oversaturated subhalocline water is entrained in the surface lens (diapycnal flux) and  
431 transported laterally out of the system in its dissolved form. During periods of low river flow, the surface lens is  
432 thinner and residence times longer (**Andrewartha and Wild-Allen 2017; Maxey et al., 2022**). We suspect that  
433 N<sub>2</sub>O from the oversaturated subhalocline water then diffuses through the surface layer and is emitted into the  
434 atmosphere in its gaseous form (**Figure** ). Our estimates of diapycnal flux indicate that the mass transport from

435 subhalocline waters is smaller (~2x smaller) than the air/sea flux, supporting this idea. This conceptual model  
436 suggests that the harbour surface lens functions to capture both gaseous N<sub>2</sub>O from the atmosphere and dissolved  
437 N<sub>2</sub>O generated in the subhalocline layer and transport it to the ocean in its dissolved form during high flow  
438 periods (**Figure** ).

439 This study focusing on characterizing N<sub>2</sub>O dynamics at end-members and at stations through the  
440 harbour's longitudinal axis. Other areas of the harbour, most prominently the shallow embayments around the  
441 parameter of the system and the areas occupied by fin fish farms were not included here. Fin fish aquaculture can  
442 increase water column DO demand near the pens in this system (**Maxey et al., 2020**), and introduces particulate  
443 organic material to the water. Whether this manifests in altered N cycling dynamics (especially DO sensitive  
444 processes like nitrification and denitrification) would be system specific and has never been described in this  
445 system. High particles loads have been shown to induce denitrification in normoxic waters *e.g.* **Wan et al.,**  
446 **(2023)**; **Frey et al., (2020)**; **Codispoti et al., (2005)**; **Nevison et al., (2003)**; **Usui et al., (2001)**; **Robinson et**  
447 **al., (1998)** so an N<sub>2</sub>O sink might be present even under farms, even in more oxygenated basins. Future studies  
448 should investigate the impacts of fin fish aquaculture on DO and N<sub>2</sub>O cycling.

449 One source of uncertainty in our approach is in using literature derived estimators for air/sea and  
450 diapycnal flux estimations. We also used literature derived  $k_{600}$  estimates from **Nightingale et al., (2000)**,  
451 **Raymond and Cole (2001)**, and **Wanninkhof (2014)** to compute N<sub>2</sub>O air/sea flux. Literature derived estimators  
452 of  $K_{600}$  and eddy diffusivity are commonly used when direct measurements are unavailable (**Tang et al., 2024**;  
453 **Li et al. 2023**; **Murray et al. 2020**) but to reduce uncertainty these are ideally measure in situ. Likewise, we  
454 presented diapycnal flux estimates using turbulent eddy diffusivities from **Fer et al., (2006)** which were not  
455 measured in Macquarie Harbour.

456 Previous work in Australian estuaries with pristine catchments (like Macquarie Harbour) has shown that  
457 many tend to function as a sink for atmospheric N<sub>2</sub>O (**Maher et al., 2016**; **Wells et al., 2018**). Our study adds  
458 the caveat that water column / atmospheric exchange may also depend on factors controlling river flow in deeper  
459 stratified systems. Despite the advancements made to date, many of the deeper estuaries in Chile, Australia and  
460 New Zealand are lacking descriptions of N<sub>2</sub>O exchange between the water column and atmosphere (*e.g.* Bathurst  
461 Harbour, Tasmania; fjords of South Island New Zealand; estuaries on Stewart Island New Zealand). Given that  
462 these systems have relatively pristine catchments they offer an opportunity to better understand natural fjord-like  
463 estuarine responses to the climate drivers of N<sub>2</sub>O dynamics. Mesoscale climate oscillations (*i.e.* the Southern  
464 Annular Mode; SAM; North Atlantic Oscillation; NAO) have been shown to affect rainfall, river flow, and DO  
465 concentrations in this and other fjord-like estuaries (**Maxey et al., 2022**; **Austin and Inall, 2002**). In Western  
466 Tasmania, SAM in its positive phase results in increased orographic rainfall and a greater propensity for higher  
467 river flow, possibly tilting the source and sink balance to net N<sub>2</sub>O uptake during these periods.

468 Climate change predictions for Tasmania's West Coast (which includes the Macquarie Harbour  
469 catchment) indicate that the region will experience a more extreme precipitation regime with increased winter  
470 precipitation and decreased summer precipitation (**Grose et al., 2010**; **Bennett et al., 2010**). If these future  
471 predictions result in more extreme seasonality in Gordon River flow, then the harbour may respond in kind with  
472 a larger variation in N<sub>2</sub>O air / sea flux *i.e.* greater N<sub>2</sub>O atmospheric uptake in winter and greater N<sub>2</sub>O emission in  
473 summer. However, given that the river flow is somewhat regulated by the hydroelectric dam, our study suggests  
474 that flow regulation has the potential to augment harbour N<sub>2</sub>O emissions. Releasing water during extreme low

475 rainfall periods might allow N<sub>2</sub>O slowly accumulating in subhalocline waters to be released in the exported  
476 surface lens.

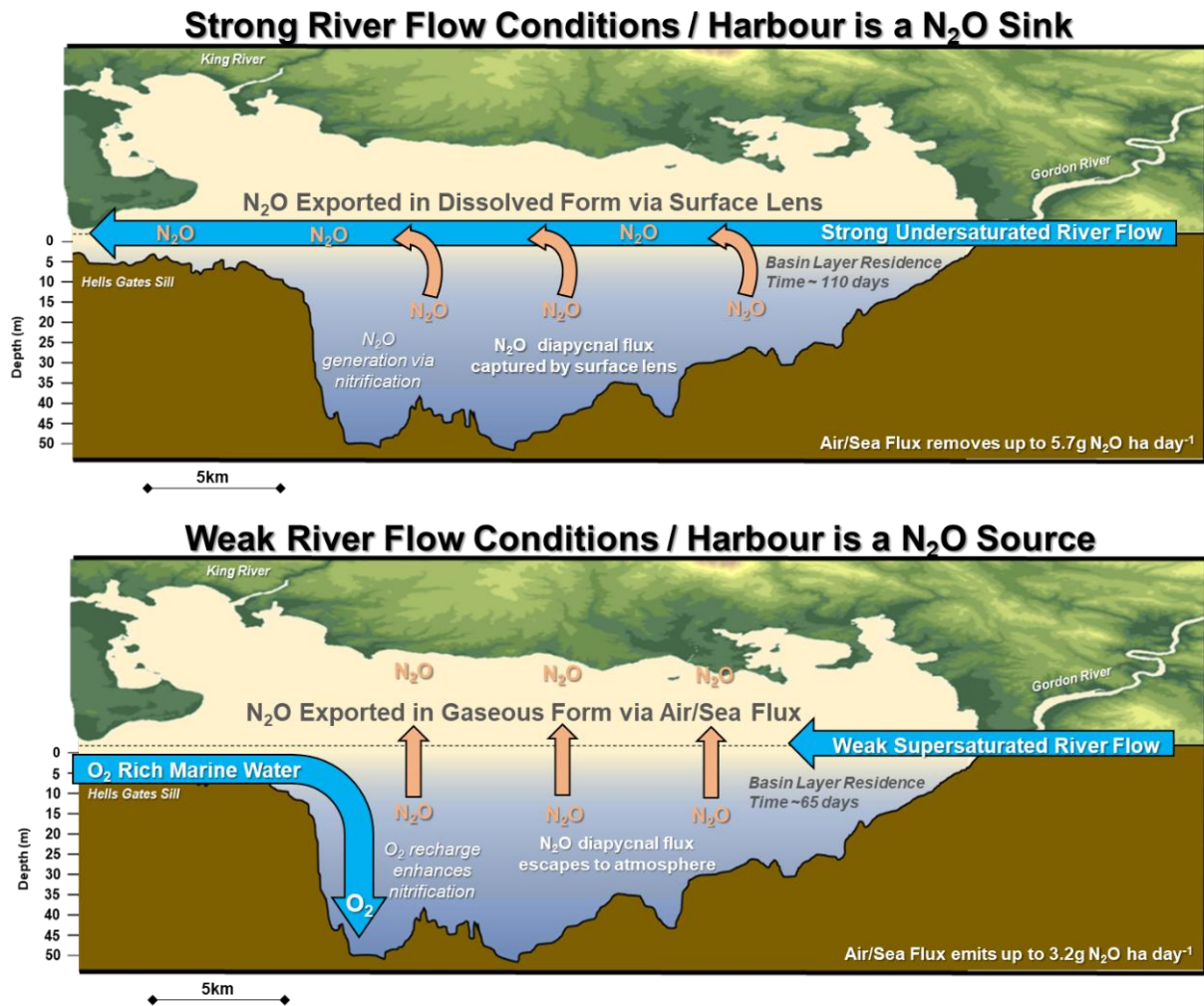
477 It is well established that fjord and fjord-like estuaries are important sites of C burial (**Smith *et al.*,**  
478 **2015; Bianchi *et al.*, 2018, 2020**). This study supports the idea that they can also be important sites of  
479 atmospheric N<sub>2</sub>O removal and transport. Macquarie Harbour air/sea flux estimates are similar in magnitude to  
480 observations made in other stratified estuaries and enclosed seas such as the Reloncaví Estuary, Chile (**Yevenes**  
481 ***et al.*, 2017**) and Eckernförde Bay, Germany (**Ma *et al.*, 2019**) (**Table A1**). Macquarie Harbour, however, was  
482 observed to have lower fluxes of N<sub>2</sub>O into the atmosphere than other river dominated, but not fjord-like,  
483 estuaries (Elbe River, Germany; **Schulz *et al.*, 2023**) including those on the Australian mainland's east coast  
484 (**Wells *et al.*, 2018**).

485 Fjord and fjord-like estuaries are defined by their strong stratification and sensitivity to freshwater  
486 inputs. With climate change, rainfall patterns are expected to become more extreme and thus alter the river flow,  
487 and subsequently N<sub>2</sub>O source sink dynamics in these systems on a global scale. In systems that are expected to  
488 experience increasingly drier conditions they may shift from net sinks of N<sub>2</sub>O to sources, and further perpetuate  
489 the accumulation of N<sub>2</sub>O in the atmosphere.

## 490 **5. Conclusions**

491 In summary, river flow, and specifically river flow driven by hydroelectric dam release, significantly affects both  
492 surface water N<sub>2</sub>O concentrations and air/sea flux in Macquarie Harbour. Importantly, when river flow is low  
493 most of the harbour emits N<sub>2</sub>O to the atmosphere. When river flow is high most of the harbour removes N<sub>2</sub>O  
494 from the atmosphere, intercepts the diapycnal flux, and laterally exports this N<sub>2</sub>O to the ocean in its dissolved  
495 form. N<sub>2</sub>O is continually supersaturated below the halocline and the relationship between AOU and ΔN<sub>2</sub>O and  
496 N<sub>2</sub>O saturation and NO<sub>3</sub><sup>-</sup> concentration indicates that the main N<sub>2</sub>O generation process is likely nitrification.  
497 Climate change is predicted to result in wetter winter / drier summers for the Tasmanian West Coast, which may  
498 result in augmented N<sub>2</sub>O air/sea fluxes. This work represents the first descriptions of N<sub>2</sub>O spatiotemporal  
499 distribution, estimated air/sea flux, estimated diapycnal flux, and N<sub>2</sub>O production pathways in this system.

500



501  
 502 **Figure 9: Conceptual model of Macquarie Harbour's N<sub>2</sub>O dynamics.** The top diagram depicts the capture of N<sub>2</sub>O  
 503 generated in the subhalocline during strong river flow conditions. Here N<sub>2</sub>O is exported from the harbour in its  
 504 dissolved form via undersaturated surface flows from the harbour to the ocean. The bottom diagram depicts the  
 505 efflux of N<sub>2</sub>O from the harbour surface during low flow conditions. Note that during these conditions the surface  
 506 flows are weak and generally supersaturated with N<sub>2</sub>O permitting its escape in gaseous form to the atmosphere.

507

509 **Table A1: N<sub>2</sub>O fluxes and observed ranges of mean ( $\pm$  standard deviation) N<sub>2</sub>O concentration / saturation from both**  
510 **fjord-like / river dominated estuaries around the globe and estuaries in Australia.**

Location	System Type	Measurement Depth Range	Mean Sea-to-Air N <sub>2</sub> O flux uMol N <sub>2</sub> O m <sup>-2</sup> day <sup>-1</sup>	Min and Max Sea-to-Air N <sub>2</sub> O flux uMol N <sub>2</sub> O m <sup>-2</sup> day <sup>-1</sup>	Mean N <sub>2</sub> O Concentration (and Saturation) nM N <sub>2</sub> O (and %)	Min and Max N <sub>2</sub> O Concentration (and Saturation) nM N <sub>2</sub> O (and %)	Reference
Macquarie Harbour, Western Tasmania, Australia	Fjord-like Estuary	2m to 45m	-09.83 $\pm$ 0.67 to 05.65 $\pm$ 1.22	-10.82 to 7.73	11.7 $\pm$ 1.6 (121.8 $\pm$ 17.8)	7.87 to 17.12 (81 to 174)	<i>This Study</i>
Reloncaví Estuary, Chile	Fjord-like Estuary	0m to 5m	0.86 $\pm$ 2.28	-1.58 to 5.60	11.8 $\pm$ 1.70 (111 $\pm$ 18.3)	8.34 to 14.5 (80 to 140)	Yevenes <i>et al.</i> , 2017
Reloncaví Estuary, Chile	Fjord-like Estuary	10m to 200m	-	-	14.5 $\pm$ 1.73 (145 $\pm$ 17.7)	10.5 to 17.0 (11 to 170)	Yevenes <i>et al.</i> , 2017
Chiloé Interior Sea, Chile	Fjord-like Estuary	0m to 200m	1.08 $\pm$ 1.41	-0.18 to 3.19	12.6 $\pm$ 2.36 (121 $\pm$ 17.5)	8.81 to 21.1 (87 to 160)	Yevenes <i>et al.</i> , 2017
Europa Sound, Magellanic Region, Chile	Fjord-like Estuary	1m to 10m	-15.22 to -0.81	-	11.9 $\pm$ 5.7 to 12.7 $\pm$ 1.0	-	Farías <i>et al.</i> , 2018
Concepción Channel, Magellanic Region, Chile	Fjord-like Estuary	1m to 150m	0.69 to 7.70	-	13.6 $\pm$ 1.1 to 17.0 $\pm$ 0.02	-	Farías <i>et al.</i> , 2018
Sarmiento Channel, Magellanic Region, Chile	Fjord-like Estuary	1m to 10m	2.07 to 12.53	-	13.1 $\pm$ 0.1 to 16.5 $\pm$ 0.3	-	Farías <i>et al.</i> , 2018
Estero Peel, Magellanic Region, Chile	Fjord-like Estuary	1m to 10m	0.11 to 2.01	-	13.1 $\pm$ 0.2 to 13.5 $\pm$ 0.5	-	Farías <i>et al.</i> , 2018
Estero Calvo, Magellanic Region, Chile	Fjord-like Estuary	1m to 10m	0.04	-	13.9 $\pm$ 0.8	-	Farías <i>et al.</i> , 2018
Estero Amalia, Magellanic Region, Chile	Fjord-like Estuary	1m to 100m	-0.08	-	14.2 $\pm$ 1.7	-	Farías <i>et al.</i> , 2018
Estero las Montañas, Magellanic Region, Chile	Fjord-like Estuary	1m to 10m	-2.95	-	9.69 $\pm$ 1.6	-	Farías <i>et al.</i> , 2018
Smyth Channel, Magellanic Region, Chile	Fjord-like Estuary	1m to 300m	1.07 to 11.2	-	14.3 $\pm$ 0.4 to 16.0 $\pm$ 0.5	-	Farías <i>et al.</i> , 2018
Última Esperanza Sound, Magellanic Region, Chile	Fjord-like Estuary	1m to 10m	-3.7 to 10.4	-	12.1 $\pm$ 1.1 to 13.7 $\pm$ 0.07	-	Farías <i>et al.</i> , 2018
Almirante Montt Gulf, Magellanic Region, Chile	Fjord-like Estuary	1m to 150m	15.6	-	21.0 $\pm$ 5.7	-	Farías <i>et al.</i> , 2018
Kirke Channel, Magellanic Region, Chile	Fjord-like Estuary	1m to 10m	0.12 to 8.19	-	13.3 $\pm$ 0.1 to 15.4 $\pm$ 0.4	-	Farías <i>et al.</i> , 2018
Union Channel, Magellanic Region, Chile	Fjord-like Estuary	1m to 10m	22.1	-	16.7 $\pm$ 0.8	-	Farías <i>et al.</i> , 2018
Union Sound, Magellanic Region, Chile	Fjord-like Estuary	1m to 10m	2.86	-	14.8 $\pm$ 0.8	-	Farías <i>et al.</i> , 2018
Western Magellan Strait, Magellanic Region, Chile	Fjord-like Estuary	1m to 10m	143	-	15.71	-	Farías <i>et al.</i> , 2018
Eastern Magellan Strait, Magellanic Region, Chile	Fjord-like Estuary	1m	36.3	-	16.4	-	Farías <i>et al.</i> , 2018
San Gregorio Cape, Magellanic Region, Chile	Fjord-like Estuary	1m	24.8	-	12.07	-	Farías <i>et al.</i> , 2018
Otway Center Sound, Magellanic Region, Chile	Fjord-like Estuary	1m	35.5	-	11.4	-	Farías <i>et al.</i> , 2018
Magdalena North Channel, Magellanic Region, Chile	Fjord-like Estuary	1m	-0.22	-	11.4	-	Farías <i>et al.</i> , 2018
Chasco Sound, Magellanic Region, Chile	Fjord-like Estuary	1m	6.81	-	16.01	-	Farías <i>et al.</i> , 2018
Cockburn West Channel, Magellanic Region, Chile	Fjord-like Estuary	1m	6.18	-	14.47	-	Farías <i>et al.</i> , 2018
Saanich Inlet, British Columbia, Canada	Fjord-like Estuary	10m to 200m	2.3 $\pm$ 2.5 to 3.9 $\pm$ 2.9	-	14.7	<0.5 to 37.4	Capelle <i>et al.</i> , 2018
Saanich Inlet, British Columbia, Canada	Fjord-like Estuary	Surface to 110m	11.3 to 20.4	-	-	-	Cohen 1978
Elbe River Estuary, Germany	Well-Mixed River Dominated Estuary	1.2m	-	26.0 $\pm$ 23.5 to 100.7 $\pm$ 101.2	-	(161 $\pm$ 53.6) to (243 $\pm$ 141.6)	Schulz <i>et al.</i> 2023
Eckernförde Bay, Boknis Eck Time Series Station, Baltic Sea, Germany	Enclosed Sea	1m to 25m	3.5 $\pm$ 12.4	-19.0 to 105.7	(111 $\pm$ 30)	(56 to 314)	Ma <i>et al.</i> , 2019
Eckernförde Bay, Boknis Eck Time Series Station, Baltic Sea, Germany	Enclosed Sea	1m to 25m	-	-	10 to 17	-	Walter <i>et al.</i> , 2006
Baltic Sea, Germany	Enclosed Sea	110m	5 -11	-	14 to 1523	-	Rönner 1983



Gotland Basin, Baltic Sea, Germany	Enclosed Sea	90m	-	-	13	0 to 126 (0 to 450)	Brettar and Rheinheimer 1991
Northwest Shelf, Black Sea	Enclosed Sea	-	1.6 to 4.4	-	6.5 to 8	-	Amouroux <i>et al.</i> , 2002
Deep Basin, Black Sea	Enclosed Sea	70m	3.1 to 5.2	-	7.5 to 10.2	-	Amouroux <i>et al.</i> , 2002
Cariaco Basin, Venezuela	Coastal Basin	Surface to 400m	-	-	4.4 to 5.5	-	Hashimoto <i>et al.</i> , 1983
Guadalquivir Estuary, Gulf of Cadiz, Spain	River Dominated Estuary	2m	18.7 ± 33.6	-	20.6 ± 24.3	-	Sierra <i>et al.</i> , 2020
Guadalquivir Estuary, Gulf of Cadiz, Spain	River Dominated Estuary	2m	0.3 ± 0.5	-	6.7 ± 0.4	-	Sierra <i>et al.</i> , 2020
Guadalquivir Estuary, Gulf of Cadiz, Spain	River Dominated Estuary	2m	0.9 ± 21.6	-	7.3 ± 15.4	-	Sierra <i>et al.</i> , 2020
Noosa River Estuary, Eastern Australia	River Dominated Estuary	0.5m to 9.6m	-14.24 ± 14.02	-57.72 to 22.20	6.99 ± 0.43 (97 ± 2.2)	5.92 to 7.95 (90 to 103)	Wells <i>et al.</i> , 2018
Mooloolah River Estuary, Eastern Australia	River Dominated Estuary	0.5m to 6.8m	-7.33 ± 7.25	-48.76 to 16.31	6.74 ± 0.64 (97 ± 3.8)	5.19 to 7.71 (82 to 112)	Wells <i>et al.</i> , 2018
Maroochy River Estuary, Eastern Australia	River Dominated Estuary	0.5m to 8.2m	51.33 ± 55.3	-34.94 to 179.64	8.4 ± 1.50 (113 ± 16.7)	6.07 to 12.93 (92 to 163)	Wells <i>et al.</i> , 2018
Pine River Estuary, Eastern Australia	River Dominated Estuary	0.5m to 10.1m	17.10 ± 39.44	-33.22 to 145.50	7.1 ± 0.76 (102 ± 6.24)	6.05 to 8.57 (93 to 117)	Wells <i>et al.</i> , 2018
Brisbane River Estuary, Eastern Australia	River Dominated Estuary	0.5m to 23.9m	209.54 ± 143.59	15.42 to 662.62	9.8 ± 1.36 (133 ± 9.9)	6.75 to 12.75 (105 to 158)	Wells <i>et al.</i> , 2018
Middle Reach, Brisbane River Estuary, Eastern Australia	River Dominated Estuary	Surface	14.5 ± 1.19	5.4 ± 0.34 to 25.2 ± 1.87	-	13.1 to 17.9 (160 to 250)	Sturm <i>et al.</i> , 2017
Lower Reach, Brisbane River Estuary, Eastern Australia	River Dominated Estuary	Surface	6. ± 0.51	3.7 ± 0.85 to 9.1 ± 1.19	-	9.2 to 12.7 (125 to 410)	Sturm <i>et al.</i> , 2017
Oxley Creek, Eastern Australia	River Dominated Estuary	2.1m to 13.1m	210.59 ± 60.23	91.54 to 280.16	11.7 ± 1.34 (156 ± 19.7)	9.65 to 14.89 (139 to 199.7)	Wells <i>et al.</i> , 2017
Nerang River Estuary, Eastern Australia	River Dominated Estuary	0.5m to 6.8m	-0.62 ± 20.87	-67.98 to 45.92	6.73 ± 0.43 (100 ± 4.3)	5.99 to 7.79 (88 to 109)	Wells <i>et al.</i> , 2018
Logan River Estuary, Eastern Australia	-	0.5m to 14.4m	110.00 ± 153.55	-54.48 to 796.00	9.3 ± 2.36 (127 ± 27.5)	5.54 to 14.8 (81 to 191)	Wells <i>et al.</i> , 2018
Albert River Estuary, Eastern Australia	-	1.1m to 15.7m	90.05 ± 73.32	-9.50 to 264.25	10.10 ± 2.24 (131 ± 29.8)	7.32 to 15.1 (98 to 205)	Wells <i>et al.</i> , 2018
Darwin Creek, Australia	Mangrove Creek	~1m	-0.12	-	6.3 (98.9)	6.0 to 6.8 (95 to 104)	Maher <i>et al.</i> , 2016
Hinchinbrook Creek, Australia	Mangrove Creek	~1m	-3.43	-	6.1 (83.3)	5.6 to 6.8 (75 to 91)	Maher <i>et al.</i> , 2016
Melbourne Creek, Australia	Mangrove Creek	~1m	-1.33	-	7.9 (96.6)	6.9 to 9.1 (86 to 115)	Maher <i>et al.</i> , 2016
Morton Bay Creek, Australia	Mangrove Creek	~1m	-3.19	-	5.1 (77.4)	3.4 to 6.6 (50 to 105)	Maher <i>et al.</i> , 2016
Seventeen Seventy Creek, Australia	Mangrove Creek	~1m	-1.75	-	7.7 (94.3)	7.1 to 8.9 (88 to 106)	Maher <i>et al.</i> , 2016
Brisbane River, Australia	-	-	-	-	(285)	(135 to 435)	Musenze <i>et al.</i> , 2014
Coffs Creek, Australia	-	-	-	-	(219 ± 37)	(53 to 386)	Reading <i>et al.</i> , 2017
Coffs Creek, Australia	-	-	-	-	(266.5 ± 128)	(86 to 678)	Reading <i>et al.</i> , 2020
Boambee Creek, Australia	-	-	-	-	(197.1 ± 75)	(87 to 329)	Reading <i>et al.</i> , 2020
Bonville Creek, Australia	-	-	-	-	(183.7 ± 65)	(78 to 310)	Reading <i>et al.</i> , 2020
Pine Creek, Australia	-	-	-	-	(194.1 ± 65)	(79 to 382)	Reading <i>et al.</i> , 2020
Yarra River, Australia	Salt Wedge Estuary	-	-	-	(135.9 ± 31)	-	Tait <i>et al.</i> , 2017

511 **7. Acknowledgments**

512 We would like to thank GEOMAR for providing the facilities and training (thank you Lea, Florian, and  
513 Chukwudi) required to analyse N<sub>2</sub>O samples. We want to thank Torsten and Leonie Schwoch for their sampling  
514 assistance and tireless vessel operation on the Harbour. We want to thank the ADS Environmental Services *Sdn.*  
515 *Bhd.* technical staff for helping to collect portions of this dataset (Grace, Shukry, Atika, Chance, Gene, and  
516 Azza). We would also like to thank our families for supporting our long days away from home. This research has  
517 been supported by internal funding from ADS Environmental Services, Swinburne University of Technology  
518 student travel grant, and GEOMAR. We have used some of the data available in the MEMENTO database. The  
519 MEMENTO database is administered by the Kiel Data Management Team at GEOMAR Helmholtz Centre for  
520 Ocean Research Kiel. The database is accessible through the MEMENTO webpage: <https://memento.geomar.de>.

521 **8. Data Availability**

522 This data set is available upon request

523 **9. Author Contributions**

524 **Johnathan Daniel Maxey** – *Conceptualization, Field Collection, Analytical Methodology, Data*  
525 *Analysis, Writing – Original Draft, Writing – Review & Editing*

526

527 **Neil David Hartstein** – *Conceptualization, Field Collection, Analytical Guidance, Writing – Review &*  
528 *Editing, Funding*

529

530 **Hermann W. Bange** – *Conceptualization, Analytical Methodology, Data Analysis, Writing – Review*  
531 *& Editing*

532

533 **Moritz Müller** – *Conceptualization, Field Collection, Analytical Guidance, Writing – Review &*  
534 *Editing*

535

536 **10. Competing Interests**

537 HWB serves on the editorial board for Biogeosciences. The authors declare that they have no other conflicts of  
538 interest.

539

540 **11. References**

541 Borges, A. V., Delille, B., Schiettecatte, L. S., Gazeau, F., Abril, G., and Frankignoulle, M.: Gas transfer  
542 velocities of CO<sub>2</sub> in three European estuaries (Randers Fjord, Scheldt, and Thames). *Limnology and*  
543 *Oceanography*, 49(5), 1630-1641, 2004. DOI: 10.4319/lo.2004.49.5.1630

544

545 Acuña-González, J. A., Vargas-Zamora, J. A., and Córdoba-Muñoz, R.: A snapshot view of some vertical  
546 distributions of water parameters at a deep (200 m) station in the fjord-like Golfo Dulce, embayment, Costa Rica.  
547 *Revista de Biología Tropical*, 54(1), 193-200, 2006. ISSN: 0034-7744

548

549 Amouroux, D., Roberts, G., Rapsomanikis, S., and Andreae, M. O.: Biogenic gas (CH<sub>4</sub>, N<sub>2</sub>O, DMS) emission to  
550 the atmosphere from near-shore and shelf waters of the north-western Black Sea. *Estuarine, Coastal and Shelf*  
551 *Science*, 54(3), 575-587, 2002. DOI: 10.1006/ecss.2000.0666

552

553 Andrewartha, J. and Wild-Allen, K.: CSIRO Macquarie Harbour Hydrodynamic and Oxygen Tracer Modelling.  
554 Progress report to FRDC 2016/067 Project Steering Committee, 2017.  
555

556 Arneborg, L., Janzen, C., Liljebladh, B., Rippeth, T. P., Simpson, J. H., and Stigebrandt, A.: Spatial variability of  
557 diapycnal mixing and turbulent dissipation rates in a stagnant fjord basin. *Journal of Physical Oceanography*,  
558 34(7), 1679-1691, 2004. DOI: 10.1175/1520-0485(2004)034<1679:SVODMA>2.0.CO;2  
559

560 Austin, W. E., and Inall, M. E.: Deep-water renewal in a Scottish fjord: temperature, salinity and oxygen  
561 isotopes. *Polar Research*, 21(2), 251-257, 2002. DOI: 10.3402/polar.v21i2.6485  
562

563 Bange, H. W., Rapsomanikis, S., and Andreae, M. O.: Nitrous oxide in coastal waters. *Global Biogeochemical*  
564 *Cycles*, 10(1), 197-207, 1996. DOI: 10.1029/95GB03834.  
565

566 Bange, H. W.: Nitrous oxide and methane in European coastal waters. *Estuarine, Coastal and Shelf Science*,  
567 70(3), 361-374, 2006. DOI: 10.1016/j.ecss.2006.05.042  
568

569 Bange, H. W., Bell, T. G., Cornejo, M., Freing, A., Uher, G., Upstill-Goddard, R. C., and Zhang, G. L.:  
570 MEMENTO: A proposal to develop a database of marine nitrous oxide and methane measurements.  
571 *Environmental Chemistry*, 6, 195-197, 2009. DOI: 10.1071/en09033.  
572

573 Bange, H. W., Sim, C. H., Bastian, D., Kallert, J., Kock, A., Mujahid, A., and Müller, M.: Nitrous oxide (N<sub>2</sub>O)  
574 and methane (CH<sub>4</sub>) in rivers and estuaries of northwestern Borneo. *Biogeosciences*, 16(22), 4321-4335, 2019.  
575 DOI: 10.5194/bg-16-4321-2019  
576

577 Bange, H. W., Mongwe, P., Shutler, J. D., Arévalo-Martínez, D. L., Bianchi, D., Lauvset, S. K., Liu, C., Löscher,  
578 C. R., Martins, H., Rosentreter, J. A., Schmale, O., Steinhoff, T., Upstill-Goddard, R. C., Wanninkhof, R.,  
579 Wilson, S. T., and Xie, H.: Advances in understanding of air–sea exchange and cycling of greenhouse gases in  
580 the upper ocean, *Elementa: Science of the Anthropocene*, 12, 2024. DOI: 10.1525/elementa.2023.00044  
581

582 Bastian, D.: N<sub>2</sub>O und CH<sub>4</sub> Verteilung in Ästuaren und Flüssen im Nordwesten von Borneo, 2017. BSc thesis,  
583 Kiel University, Kiel, 50 pp., 2017.  
584

585 Baulch, H. M., Schiff, S. L., Maranger, R., and Dillon, P. J.: Nitrogen enrichment and the emission of nitrous  
586 oxide from streams. *Global Biogeochemical Cycles*, 25(4), 2011. DOI: 10.1029/2011GB004047  
587

588 Beaulieu, J. J., Shuster, W. D., and Rebholz, J. A.: Controls on gas transfer velocities in a large river. *Journal of*  
589 *Geophysical Research: Biogeosciences*, 117(G2), 2012. DOI: 10.1029/2011JG001794  
590

591 Bennett, J. C., Ling, F. L. N., Graham, B., Grose, M. R., Corney, S. P., White, C. J., Holz, G. K., Post, D. A.,  
592 Gaynor, S. M. and Bindoff, N. L.: Climate Futures for Tasmania: water and catchments technical report.

593 Antarctic Climate & Ecosystems Cooperative Research Centre, Hobart, Tasmania, 2010. ISBN: 978-1-921197-  
594 06-8  
595

596 Bianchi, T. S., Cui, X., Blair, N. E., Burdige, D. J., Eglinton, T. I., and Galy, V.: Centers of organic carbon burial  
597 and oxidation at the land-ocean interface. *Organic Geochemistry*, 115, 138-155, 2018. DOI:  
598 10.1016/j.orggeochem.2017.09.008  
599

600 Bianchi, T. S., Arndt, S., Austin, W. E., Benn, D. I., Bertrand, S., Cui, X., Faust, J., Kozirowska-Makuch, K.,  
601 Moy, C., Savage, C., Smeaton, C., Smith, R., and Syvitski, J.: Fjords as aquatic critical zones (ACZs). *Earth-*  
602 *Science Reviews*, 203(103145), 2020. DOI: 10.1016/j.earscirev.2020.103145  
603

604 Brase, L., Bange, H. W., Lendt, R., Sanders, T., and Dähnke, K.: High resolution measurements of nitrous oxide  
605 (N<sub>2</sub>O) in the Elbe estuary. *Frontiers in Marine Science*, 4(162), 2017. DOI: 10.3389/fmars.2017.00162  
606

607 Breider, F., Yoshikawa, C., Makabe, A., Toyoda, S., Wakita, M., Matsui, Y., Kawagucci, S., Fujiki, T., Harada,  
608 N. and Yoshida, N.: Response of N<sub>2</sub>O production rate to ocean acidification in the western North Pacific. *Nature*  
609 *Climate Change*, 9(12), 954-958, 2019. DOI: 10.1038/s41558-019-0605-7  
610

611 Breitburg, D., Grégoire, M., and Isensee, K. (eds): Global Ocean Oxygen Network 2018. The ocean is losing its  
612 breath: Declining oxygen in the world's ocean and coastal waters. OC-UNESCO, IOC Technical Series, No. 137,  
613 2018.  
614

615 Brettar, I., and Rheinheimer, G.: Denitrification in the Central Baltic: evidence for H<sub>2</sub>S-oxidation as motor of  
616 denitrification at the oxic-anoxic interface. *Marine Ecology Progress Series*, 77(2-3), 157-169, 1991.  
617 <http://www.jstor.org/stable/24826569>  
618

619 Bourbonnais, A., Lehmann, M. F., Hamme, R. C., Manning, C. C., and Juniper, S. K.: Nitrate elimination and  
620 regeneration as evidenced by dissolved inorganic nitrogen isotopes in Saanich Inlet, a seasonally anoxic fjord.  
621 *Marine Chemistry*, 157, 194–207, 2013. DOI: 10.1016/j.marchem.2013.09.006  
622

623 Capelle, D. W., Hawley, A. K., Hallam, S. J., and Tortell, P. D.: A multi-year time-series of N<sub>2</sub>O dynamics in a  
624 seasonally anoxic fjord: Saanich Inlet, British Columbia. *Limnology and Oceanography*, 63(2), 524-539, 2018.  
625 DOI: 10.1002/lno.10645  
626

627 Carpenter, P. D., Butler, E. C. V., Higgins, H. W., Mackey, D. J., and Nichols, P. D.: Chemistry of trace  
628 elements, humic substances and sedimentary organic matter in Macquarie Harbour, Tasmania. *Marine and*  
629 *Freshwater Research*, 42(6), 625-654, 1991. DOI: 10.1071/MF9910625  
630

631 Chen, C., Pan, J., Xiao, S., Wang, J., Gong, X., Yin, G., Hou, L., Liu, M., and Zheng, Y.: Microplastics alter  
632 nitrous oxide production and pathways through affecting microbiome in estuarine sediments. *Water Research*  
633 221(118733), 2022. DOI: 10.1016/j.watres.2022.118733  
634

635 Chen, J., Wells, N. S., Erler, D. V., and Eyre, B. D.: Land-use intensity increases benthic N<sub>2</sub>O emissions across  
636 three sub-tropical estuaries. *Journal of Geophysical Research: Biogeosciences* 127, 2022. DOI:  
637 10.1029/2022JG006899  
638

639 Cresswell, G. R., Edwards, R. J., Barker, B. A.: Macquarie Harbour, Tasmania-seasonal oceanographic  
640 surveys in 1985. University of Tasmania Journal contribution. 1989. DOI: 10.26749/rstpp.123.63  
641

642 de Bie, M. J. M.: Factors controlling nitrification and nitrous oxide production in the Schelde estuary. Doctoral  
643 dissertation, Yerseke: Netherlands Institute of Ecology (NIOO-CEMO). 2002.  
644

645 Dey, R., Lewis, S. C., Arblaster, J. M., and Abram, N. J.: A review of past and projected changes in Australia's  
646 rainfall. *Wiley Interdisciplinary Reviews: Climate Change*, 10(3), e577, 2019. DOI: 10.1002/wcc.577  
647

648 Etminan, M., Myhre, G., Highwood, E. J., and Shine, K. P.: Radiative forcing of carbon dioxide, methane, and  
649 nitrous oxide: A significant revision of the methane radiative forcing. *Geophysical Research Letters*, 43(24), 12-  
650 614, 2016. DOI: 10.1002/2016GL071930  
651

652 Eyring, V., Gillett, N. P., Achuta Rao, K. M., Barimalala, R., Barreiro Parrillo, M., Bellouin, N., Cassou, C.,  
653 Durack, P. J., Kosaka, Y., McGregor, S., Min, S., Morgenstern, O., Sun, Y.: Human Influence on the Climate  
654 System. In *Climate Change 2021: The Physical Science Basis. Contribution of Working Group I to the Sixth*  
655 *Assessment Report of the Intergovernmental Panel on Climate Change*. Masson-Delmotte, V., Zhai, P., Pirani,  
656 A., Connors, S. L., Péan, C., Berger, S., Caud, N., Chen, Y., Goldfarb, L., Gomis, M. I., Huang, M., Leitzell,  
657 K., Lonnoy, E., Matthews, J. B. R., Maycock, T. K., Waterfield, T., Yelekçi, O., Yu, R., and Zhou, B. (eds.):  
658 Cambridge University Press, Cambridge, United Kingdom and New York, NY, USA, 423–552, 2021. DOI:  
659 10.1017/9781009157896.005.  
660

661 Farías, L., Bello, E., Arancibia, G., Fernandez, J.: Distribution of dissolved methane and nitrous oxide in Chilean  
662 coastal systems of the Magellanic Sub-Antarctic region (50°– 55°S). *Estuarine, Coastal and Shelf Science*, 215,  
663 225-240, 2018. DOI: 10.1016/j.ecss.2018.10.020.  
664

665 Fer, I.: Scaling turbulent dissipation in an Arctic fjord. *Deep Sea Research Part II: Topical Studies in*  
666 *Oceanography*, 53(1-2), 77-95, 2006. DOI: 10.1016/j.dsr2.2006.01.003  
667

668 Forster P., Storelvmo T., Armour K., Collins W., Dufresne J.-L., Frame D., Lunt, D., Mauritsen, T., Palmer, M.,  
669 Watanabe, M., Wild, M.: The earth's energy budget, climate feedbacks, and climate sensitivity In *Climate*  
670 *Change 2021: The Physical Science Basis. Contribution of Working Group I to the Sixth Assessment Report of*

671 the Intergovernmental Panel on Climate Change. Masson-Delmotte, V., Zhai, P., Pirani, A., Connors, S. L.,  
672 Péan, C., Berger, S., Caud, N., Chen, Y., Goldfarb, L., Gomis, M. I., Huang, M., Leitzell, K., Lonnoy, E.,  
673 Matthews, J. B. R., Maycock, T. K., Waterfield, T., Yelekçi, O., Yu, R., and Zhou, B. (eds.): Cambridge  
674 University Press, Cambridge, United Kingdom and New York, NY, USA, 423–552, 2021. DOI:  
675 10.1017/9781009157896.009

676

677 Gilbert, D., Rabalais, N. N., Diaz, R. J., & Zhang, J.: Evidence for greater oxygen decline rates in the coastal  
678 ocean than in the open ocean. *Biogeosciences*, 7(7), 2283-2296, 2010. DOI: 10.5194/bg-7-2283-2010

679

680 Gillibrand, P. A., Cage, A. G., and Austin, W. E. N.: A preliminary investigation of basin water response to  
681 climate forcing in a Scottish fjord: evaluating the influence of the NAO. *Continental Shelf Research*, 25(5-6),  
682 571-587, 2005. DOI: 10.1016/j.csr.2004.10.011

683

684 Grose, M. R., Barnes-Keoghan, I., Corney S. P., White C. J., Holz, G.K., Bennett, J. B., Gaynor, S.M. and  
685 Bindof, N.L.: Climate Futures for Tasmania: general climate impacts technical report, Antarctic Climate &  
686 Ecosystems Cooperative Research Centre, Hobart, Tasmania, 2010. ISBN: 978-1-921197-05-5

687

688 Hartstein, N. D., Maxey, J. D., Loo, J. C. H., and Then, A. Y. H.: Drivers of deep water renewal in Macquarie  
689 Harbour, Tasmania. *Journal of Marine Systems*, 199(103226), 2019. DOI: 10.1016/j.jmarsys.2019.103226

690

691 Hashimoto, L. K., Kaplan, W. A., Wofsy, S. C., and McElroy, M. B.: Transformations of fixed nitrogen and  
692 N<sub>2</sub>O in the Cariaco Trench. *Deep Sea Research Part A. Oceanographic Research Papers*, 30(6), 575-590, 1983.  
693 DOI: 10.1016/0198-0149(83)90037-7

694

695 Hendzel, L. L., Matthews, C. J. D., Venkiteswaran, J. J., St. Louis, V. L., Burton, D., Joyce, E. M., and Bodaly,  
696 R. A.: Nitrous oxide fluxes in three experimental boreal forest reservoirs. *Environmental Science & Technology*,  
697 39(12), 4353-4360, 2005. DOI: 10.1021/es049443j

698

699 Huang, Y., Song, B., Zhang, Q., Park, Y., Wilson, S. J., Tobias, C. R., and An, S.: Seawater intrusion effects on  
700 nitrogen cycling in the regulated Nakdong River Estuary, South Korea. *Frontiers in Marine Science*.  
701 11(1369421), 2024. DOI: 10.3389/fmars.2024.1369421

702

703 Inall, M. E., & Gillibrand, P. A.: The physics of mid-latitude fjords: a review. Geological Society, London,  
704 Special Publications. 344(1), 17-33, 2010. DOI: 10.1144/SP344.3

705

706 Ji, Q., Jameson, B. D., Juniper, S. K., and Grundle, D. S.: Temporal and vertical oxygen gradients modulate  
707 nitrous oxide production in a seasonally anoxic fjord: Saanich Inlet, British Columbia. *Journal of Geophysical*  
708 *Research: Biogeosciences*, 125(9), 2020. DOI: 10.1029/2020JG005631

709

710 Kallert, J.: Verteilung von Lachgas (N<sub>2</sub>O) und Methan (CH<sub>4</sub>) im Fluss Rajang (Malaysia). Bachelor thesis,  
711 Christian-Albrecht-University, Kiel, 2017. URI: <https://oceanrep.geomar.de/id/eprint/40913/>  
712

713 Kock, A. and Bange, H. W.: Counting the ocean's greenhouse gas emissions, *Eos: Earth & Space Science News*,  
714 96(3), 10–13, 2015. DOI:10.1029/2015EO023665  
715

716 Ku, Harry H. "Notes on the use of propagation of error formulas." *Journal of Research of the National Bureau of*  
717 *Standards* 70, no. 4 (1966). DOI: jresv70Cn4p263\_A1b  
718

719 Kuypers, M. M. M., Marchant, H. K., and Kartal, B.: The microbial nitrogen-cycling network, *Nature Reviews*  
720 *Microbiology*, 16, 263-276, 2018. DOI: 10.1038/nrmicro.2018.9  
721

722 Laffoley, D., and Baxter, J. M.: Ocean deoxygenation: Everyone's problem: Causes, impacts, consequences and  
723 solutions: Summary for Policy Makers. International Union for Conservation of Nature (IUCN), 2019. DOI:  
724 10.2305/IUCN.CH.2019.13.en  
725

726 Li, Yuhong, Yang Luo, Jian Liu, Wangwang Ye, Jiexia Zhang, and Liyang Zhan.: Sources and sinks of N<sub>2</sub>O in  
727 the subtropical Jiulong River Estuary, Southeast China. *Frontiers in Marine Science* 10 (2023): 1138258. DOI:  
728 10.3389/fmars.2023.1138258  
729

730 Limburg, Karin E., Denise Breitburg, Dennis P. Swaney, and Gil Jacinto.: Ocean deoxygenation: A primer. *One*  
731 *Earth* 2, no. 1. 2020: 24-29. DOI: 10.1016/j.oneear.2020.01.001  
732

733 Lucieer, V.: *SeaMap Tasmania Bathymetric Data* [data set], Institute for Marine and Antarctic Studies,  
734 University of Tasmania, 2007. ISBN: 0-7246-8011-X  
735

736 Ma, X., Lennartz, S. T., and Bange, H. W. : A multi-year observation of nitrous oxide at the Boknis Eck Time  
737 Series Station in the Eckernförde Bay (southwestern Baltic Sea). *Biogeosciences*, 16(20), 4097-4111, 2019.  
738 DOI: 10.5194/bg-16-4097-2019  
739

740 Macquarie Harbour Dissolved Oxygen Working Group (October 2014), Final Report to the Tasmanian Salmonid  
741 Growers Association, 2014.  
742

743 Maher, D. T., J. Z. Sippo, D. R. Tait, C. Holloway, and Santos, I. R.: Pristine mangrove creek waters are a sink  
744 of nitrous oxide. *Scientific Reports*, 6(25701), 2016. DOI: 10.1038/srep25701  
745

746 Manning, C. C., Hamme, R. C., & Bourbonnais, A.: Impact of deep-water renewal events on fixed nitrogen loss  
747 from seasonally-anoxic Saanich Inlet. *Marine Chemistry*, 122(1), 1–10, 2010. DOI:  
748 10.1016/j.marchem.2010.08.002  
749



750 Maxey, J. D., Hartstein, N. D., Penjinus, D., & Kerroux, A.: Simple quality control technique to identify  
751 dissolved oxygen diffusion issues with biochemical oxygen demand bottle incubations. *Borneo Journal of*  
752 *Marine Science and Aquaculture (BJoMSA)*, 1, 2017. DOI: 10.51200/bjomsa.v1i.995  
753  
754 Maxey, J. D., Hartstein, N. D., Then, A. Y. H., and Barrenger, M.: Dissolved oxygen consumption in a fjord-like  
755 estuary, Macquarie Harbour, Tasmania. *Estuarine, Coastal and Shelf Science*, 246(107016), 2020. DOI:  
756 10.1016/j.ecss.2020.107016  
757  
758 Maxey, J. D., Hartstein, N. D., Mujahid, A., & Müller, M.: The influence of mesoscale climate drivers on  
759 hypoxia in a fjord-like deep coastal inlet and its potential implications regarding climate change: examining a  
760 decade of water quality data. *Biogeosciences*, 19(13), 3131-3150, 2022. DOI: 10.5194/bg-19-3131-2022  
761  
762 McMahon, P. B., and Dennehy, K. F.: N<sub>2</sub>O emissions from a nitrogen-enriched river. *Environmental Science &*  
763 *Technology*, 33(1), 21-25, 1999. DOI: 10.1021/es980645n  
764  
765 Michiels, C. C., Huggins, J. A., Giesbrecht, K. E., Spence, J. S., Simister, R. L., Varela, D. E., Hallam, S. J.,  
766 Crowe, S. A.: Rates and pathways of N<sub>2</sub> production in a persistently anoxic fjord: Saanich Inlet, British  
767 Columbia. *Frontiers in Marine Science*, 6(27), 2019. DOI: 10.3389/fmars.2019.00027  
768  
769 Mickett, J. B., Gregg, M. C., and Seim, H. E.: Direct measurements of diapycnal mixing in a fjord reach—Puget  
770 Sound's Main Basin. *Estuarine, Coastal and Shelf Science*, 59(4), 539-558, 2004. DOI:  
771 10.1016/j.ecss.2003.10.009  
772  
773 Murray, R. H., Erler, D. V., and Eyre, B. D.: Nitrous oxide fluxes in estuarine environments: response to global  
774 change. *Global Change Biology*, 21(9), 3219-3245, 2015. DOI: 10.1111/gcb.12923  
775  
776 Murray, Rachel, Dirk V. Erler, Judith Rosentreter, Naomi S. Wells, and Bradley D. Eyre.: Seasonal and spatial  
777 controls on N<sub>2</sub>O concentrations and emissions in low-nitrogen estuaries: Evidence from three tropical systems.  
778 *Marine Chemistry* 221 (2020): 103779. DOI: 10.1016/j.marchem.2020.103779  
779  
780 Musenze, R. S., U. Werner, A. Grinham, J. Udy, and Z. Yuan.: Methane and nitrous oxide emissions from a  
781 subtropical estuary (the Brisbane River estuary, Australia). *Science of the Total Environment*, 472, 719–729,  
782 2014. DOI: 10.1016/j.scitotenv.2013.11.085  
783  
784 Myhre, G., Shindell, D., Bréon, F. M., Collins, W., Fuglestedt, J., Huang, J., Koch, D., Lamarque, J. F., Lee,  
785 D., Mendoza, B., Nakajima, T., Robock, A., Stephens, G., Takemura, T., and Zhang, H.: Anthropogenic and  
786 Natural Radiative Forcing. In: *Climate Change 2013: The Physical Science Basis. Contribution of Working*  
787 *Group I to the Fifth Assessment Report of the Intergovernmental Panel on Climate Change* [Stocker, T.F., Qin,  
788 D., Plattner, G. K., Tignor, M., Allen, S. K., Boschung, J, Nauels, A., Xia, Y., Bex, V., and Midgley, P. M.

789 (eds.)). Cambridge University Press, Cambridge, United Kingdom and New York, NY, USA, 2013. DOI:  
790 10.1017/CBO9781107415324.018  
791  
792 Myllykangas, J. P., Jilbert, T., Jakobs, G., Rehder, G., Werner, J., and Hietanen, S.: Effects of the 2014 major  
793 Baltic inflow on methane and nitrous oxide dynamics in the water column of the central Baltic Sea. *Earth System*  
794 *Dynamics*, 8(3), 817-826, 2017. DOI: 10.5194/esd-8-817-2017  
795  
796 Nevison, C., and Holland, E.: A reexamination of the impact of anthropogenically fixed nitrogen on atmospheric  
797 N<sub>2</sub>O and the stratospheric O<sub>3</sub> layer. *Journal of Geophysical Research: Atmospheres*, 102(D21), 25519-25536,  
798 1997. DOI: 10.1029/97JD02391  
799  
800 Orif, M. I., Yasar N. K., Radwan K. A., and Sudheesh, V.: Deoxygenation turns the coastal Red Sea lagoons into  
801 sources of nitrous oxide. *Marine Pollution Bulletin* 189(114806), 2023. DOI: 10.1016/j.marpolbul.2023.114806  
802  
803 Portmann, R. W., Daniel, J. S., and Ravishankara, A. R.: Stratospheric ozone depletion due to nitrous oxide:  
804 influences of other gases. *Philosophical Transactions of the Royal Society B*, 367, 1256–1264, 2012. DOI:  
805 10.1098/rstb.2011.0377  
806  
807 Raes, E. J., Bodrossy, L., Van de Kamp, J., Holmes, B., Hardman-Mountford, N., Thompson, P. A., McInnes, A.  
808 S., Waite, A. M.: Reduction of the powerful greenhouse gas N<sub>2</sub>O in the South-Eastern Indian Ocean. *PLoS One*,  
809 11(1), 2016. DOI: 10.1371/journal.pone.0145996  
810  
811 Ravishankara, A. R., Daniel, J. S., and Portmann, R. W.: Nitrous oxide (N<sub>2</sub>O): the dominant ozone-depleting  
812 substance emitted in the 21st century. *Science*, 326(5949), 123-125, 2009. DOI: 10.1126/science.1176985  
813  
814 Raymond, P. A., and Cole, J. J.: Gas exchange in rivers and estuaries: Choosing a gas transfer velocity.  
815 *Estuaries*, 24(2), 312-317, 2001. DOI: 10.2307/1352954  
816  
817 Reading, M. J., Santos, I. R., Maher, D. T., Jeffrey, L. C., and Tait, D. R.: 2017. Shifting nitrous oxide  
818 source/sink behaviour in a subtropical estuary revealed by automated time series observations. *Estuarine, Coastal*  
819 *and Shelf Science*, 194: 66-76, 2017. DOI: 10.1016/j.ecss.2017.05.017  
820  
821 Reading, M. J., Tait, D. R., Maher, D. T., Jeffrey, L. C., Looman, A., Holloway, C., Shishaye, H. A., Barron, S.  
822 and Santos, I. R.: Land use drives nitrous oxide dynamics in estuaries on regional and global scales. *Limnology*  
823 *and Oceanography*, 65(8), 1903-1920, 2020. DOI: 10.1002/lno.11426  
824  
825 Reading, M.J.: Aquatic nitrous oxide dynamics from rivers to reefs. Doctoral dissertation, Southern Cross  
826 University, 2022. DOI: 10.25918/thesis.197  
827

828 Resplandy, Laure, Allison Hogikyan, Jens Daniel Müller, R. G. Najjar, Hermann W. Bange, Daniele Bianchi, T.  
829 Weber, W.-J. Cai, S. C. Doney, K. Fennel, M. Gehlen, J. Hauck, F. Lacroix, P. Landschützer, C. Le Quéré, A.  
830 Roobaert, J. Schwinger, S. Berthet, L. Bopp, T. T. T. Chau, M. Dai, N. Gruber, T. Ilyina, A. Kock, M. Manizza,  
831 Z. Lachkar, G. G. Laruelle, E. Liao, I. D. Lima, C. Nissen, C. Rödenbeck, R. Sférian, K. Toyama, H. Tsujino,  
832 P. Regnier.: A synthesis of global coastal ocean greenhouse gas fluxes. *Global biogeochemical cycles* 38, no. 1  
833 2024: e2023GB007803. DOI: 10.1029/2023GB007803

834

835 Rönner, U.: Distribution, production and consumption of nitrous oxide in the Baltic Sea. *Geochimica et*  
836 *Cosmochimica Acta*, 47(12), 2179-2188, 1983. DOI: 10.1016/0016-7037(83)90041-8

837

838 Rosentreter, J. A., Wells, N. S., Ulseth, A. J., and Eyre, B. D.: Divergent gas transfer velocities of CO<sub>2</sub>, CH<sub>4</sub>, and  
839 N<sub>2</sub>O over spatial and temporal gradients in a subtropical estuary. *Journal of Geophysical Research:*  
840 *Biogeosciences*, 126(10), 2021. DOI: 10.1029/2021JG006270

841

842 Rosentreter, J.A., Laruelle, G.G., Bange, H.W., Bianchi, T.S., Busecke, J.J., Cai, W.J., Eyre, B.D., Forbrich, I.,  
843 Kwon, E.Y., Maavara, T. and Moosdorf, N.: Coastal vegetation and estuaries are collectively a greenhouse gas  
844 sink. *Nature Climate Change*, 13(6), 579-587, 2023. DOI: 10.1038/s41558-023-01682-9

845

846 Sánchez-Rodríguez, J., Sierra, A., Jiménez-López, D., Ortega, T., Gómez-Parra, A., and Forja, J.: Dynamic of  
847 CO<sub>2</sub>, CH<sub>4</sub> and N<sub>2</sub>O in the Guadalquivir estuary. *Science of The Total Environment*, 805, 2022. DOI:  
848 10.1016/j.scitotenv.2021.150193

849

850 Schulz, G., Sanders, T., Voynova, Y. G., Bange, H. W., and Dähnke, K.: Seasonal variability of nitrous oxide  
851 concentrations and emissions in a temperate estuary. *Biogeosciences*, 20(15), 3229-3247, 2023. DOI:  
852 10.5194/bg-20-3229-2023

853

854 Schweiger, B.: Messung von NH<sub>2</sub>OH in ausgewählten Seegebieten. Master thesis, Leibniz Institute of Marine  
855 Science, Kiel (IFM-GEOMAR), 2006.

856

857 Seitzinger, S. P., Kroeze, C., and Styles, R. V.: Global distribution of N<sub>2</sub>O emissions from aquatic systems:  
858 natural emissions and anthropogenic effects. *Chemosphere-Global Change Science*, 2(3-4), 267-279, 2000. DOI:  
859 10.1016/S1465-9972(00)00015-5

860

861 Sierra, A., Jiménez-López, D., Ortega, T., Gómez-Parra, A., and Forja, J.: Factors controlling the variability and  
862 emissions of greenhouse gases (CO<sub>2</sub>, CH<sub>4</sub> and N<sub>2</sub>O) in three estuaries of the Southern Iberian Atlantic Basin  
863 during July 2017. *Marine Chemistry*, 226(103867), 2020. DOI: 10.1016/j.marchem.2020.103867

864

865 Salamena, G. G., Whinney, J. C., Heron, S. F., and Ridd, P. V.: Internal tidal waves and deep-water renewal in a  
866 tropical fjord: Lessons from Ambon Bay, eastern Indonesia. *Estuarine, Coastal and Shelf Science*, 253(107291),  
867 2021. DOI: 10.1016/j.ecss.2021.107291

868  
869 Salamena, G. G., Whinney, J. C., Heron, S. F., and Ridd, P. V.: Frontogenesis and estuarine circulation at the  
870 shallow sill of a tropical fjord: Insights from Ambon Bay, eastern Indonesia. *Regional Studies in Marine Science*,  
871 56(102696), 2022. DOI: 10.1016/j.rsma.2022.102696  
872  
873 Smith, R. W., Bianchi, T. S., Allison, M., Savage, C., and Galy, V.: High rates of organic carbon burial in fjord  
874 sediments globally, *Nature Geoscience*, 8(6), 450-453, 2015. DOI: 10.1038/ngeo2421  
875  
876 Stow, C. A., Walker, J. T., Cardoch, L., Spence, P., and Geron, C.: N<sub>2</sub>O emissions from streams in the Neuse  
877 River watershed, North Carolina. *Environmental Science & Technology*, 39(18), 6999-7004, 2005. DOI:  
878 10.1021/es0500355  
879  
880 Sturm, K., Werner, U., Grinham, A., and Yuan, Z.: Tidal variability in methane and nitrous oxide emissions  
881 along a subtropical estuarine gradient. *Estuarine, Coastal and Shelf Science*, 192, 159–169, 2017. DOI:  
882 10.1016/j.ecss.2017.04.027  
883  
884 Suntharalingam, P., and Sarmiento, J. L.: Factors governing the oceanic nitrous oxide distribution: Simulations  
885 with an ocean general circulation model. *Global Biogeochemical Cycles*, 14(1), 429-454, 2000. DOI:  
886 10.1029/1999GB900032  
887  
888 Tait, D. R., Maher, D. T., Wong, W., Santos, I. R., Sadat-Noori, M., Holloway, C., and Cook, P. L. M.:  
889 Greenhouse gas dynamics in a salt-wedge estuary revealed by high resolution cavity ringdown spectroscopy  
890 observations. *Environmental Science & Technology*, 51: 13771–13778, 2017. DOI: 10.1021/acs.est.7b04627  
891  
892 Tang, Weiyi, Jeff Talbott, Timothy Jones, and Bess B. Ward: Variable contribution of wastewater treatment  
893 plant effluents to downstream nitrous oxide concentrations and emissions. *Biogeosciences* 21, no. 14, 3239-3250,  
894 2024. DOI: 10.5194/bg-21-3239-2024  
895  
896 Teasdale, P. R., Apte, S. C., Ford, P. W., Batley, G. E., and Koehnken, L.: Geochemical cycling and speciation  
897 of copper in waters and sediments of Macquarie Harbour, Western Tasmania. *Estuarine, Coastal and Shelf*  
898 *Science*, 57(3), 475-487, 2003. DOI: 10.1016/S0272-7714(02)00381-5  
899  
900 Testa, Jeremy M., Jacob Carstensen, Arnaud Laurent, and Ming Li.: Hypoxia and Climate Change in Estuaries.  
901 In *Climate Change and Estuaries*, pp. 143-170. CRC Press, 2023. ISBN: 9781003126096  
902  
903 Walinsky, S. E., Prahl, F. G., Mix, A. C., Finney, B. P., Jaeger, J. M., and Rosen, G. P.: Distribution and  
904 composition of organic matter in surface sediments of coastal Southeast Alaska, *Continental Shelf Research*,  
905 29(13), 1565-1579, 2009. DOI: 10.1016/j.csr.2009.04.006  
906

907 Walter, S., Bange, H. W., and Wallace, D. W.: Nitrous oxide in the surface layer of the tropical North Atlantic  
908 Ocean along a west to east transect. *Geophysical Research Letters*, 31(23), 2004. DOI: 10.1029/2004GL019937  
909

910 Walter, S., Breitenbach, U., Bange, H. W., Naucsh, G., and Wallace, D. W. R.: Distribution of N<sub>2</sub>O in the Baltic  
911 Sea during transition from anoxic to oxic conditions. *Biogeosciences*, 3, 557-570, 2006. DOI: 10.5194/bg-3-557-  
912 2006  
913

914 Wan, X. S., Lin, H., Ward, B. B., Kao, S., and Dai M.: Significant seasonal N<sub>2</sub>O dynamics revealed by multi-  
915 year observations in the Northern South China Sea. *Global Biogeochemical Cycles*, 36(10), 2022. DOI:  
916 10.1029/2022GB007333  
917

918 Weiss, R. F. and Price, B. A.: Nitrous oxide solubility in water and seawater, *Marine Chemistry*, 8, 347-359,  
919 1980. DOI: 10.1016/0304-4203(80)90024-9  
920

921 Wells, N. S., Maher, D. T., Erler, D. V., Hipsey, M., Rosentreter, J. A., and Eyre, B. D.: Estuaries as sources and  
922 sinks of N<sub>2</sub>O across a land use gradient in subtropical Australia. *Global Biogeochemical Cycles*, 32, 877–894,  
923 2918. DOI: 10. 1029/2017GB005826  
924

925 Willis, M.: Tascatch Variation 2 – Surface Water Models (Document ID Number WR 2008/005). Department of  
926 Primary Industries and Water. Hydro Tasmania Consulting, [https://nre.tas.gov.au /water/water-monitoring-and-  
927 assessment/hydrological assessment/tasmanian-catchmentsmodelling /surface-water-models](https://nre.tas.gov.au /water/water-monitoring-and-assessment/hydrological%20assessment/tasmanian-catchmentsmodelling /surface-water-models). 2008.  
928

929 Wilson, S. T., Bange, H. W., Arévalo-Martínez, D. L., Barnes, J., Borges, A. V., Brown, I., Bullister, J. L.,  
930 Burgos, M., Capelle, D. W., Casso, M., de la Paz, M., Farías, L., Fenwick, L., Ferrón, S., Garcia, G., Glockzin,  
931 M., Karl, D. M., Kock, A., Laperriere, S., Law, C. S., Manning, C. C., Marriner, A., Myllykangas, J. P., Pohlman,  
932 J. W., Rees, A. P., Santoro, A. E., Tortell, P. D., Upstill-Goddard, R. C., Wisegarver, D. P., Zhang, G. L., and  
933 Rehder, G.: An intercomparison of oceanic methane and nitrous oxide measurements, *Biogeosciences*, 15, 5891-  
934 5907, 2018. DOI: 10.5194/bg-15-5891-2018  
935

936 Wilson, S. T., Al-Haj, A. N., Bourbonnais, A., Frey, C., Fulweiler, R. W., Kessler, J. D., Marchant, H. K.,  
937 Milucka, J., Ray, N. E., Suntharalingham, P., Thornton, B. F., Upstill-Goddard, R. C., Weber, T. S., Arévalo-  
938 Martínez, D. L., Bange, H. W., Benway, H. M., Bianchi, D., Borges, A. V., Chang, B. X., Crill, P. M., del Valle,  
939 D. A., Farías, L., Joye, S. B., Kock, A., Labidi, J., Manning, C. C., Pohlman, J. W., Rehder, G., Sparrow, K. J.,  
940 Tortell, P. D., Treude, T., Valentine, D. L., Ward B. B., Yang, S., and Yurganov, L. N.: Ideas and perspectives:  
941 A strategic assessment of methane and nitrous oxide measurements in the marine environment. *Biogeosciences*,  
942 17, 5809-5828, 2020. DOI: 10.5194/bg-17-5809-2020  
943

944 Wu, L., Chen X., Wei, W., Liu, Y., Wang, D., and Ni, B.: A critical review on nitrous oxide production by  
945 ammonia-oxidizing archaea. *Environmental Science & Technology* 54(15), 9175-9190, 2020. DOI:  
946 10.1021/acs.est.0c03948

947  
948 Yevenes, M. A., Bello, E., Sanhueza-Guevara, S., and Farías, L.: Spatial distribution of nitrous oxide (N<sub>2</sub>O) in  
949 the Reloncaví estuary–sound and adjacent sea (41–43 S), Chilean Patagonia. *Estuaries and Coasts*, 40, 807-821,  
950 2017. DOI: 10.1007/s12237-016-0184-z  
951  
952 Yoshinari, T.: Nitrous oxide in the sea. *Marine Chemistry* 2(4), 189–202, 1976. DOI: 10.1016/0304-  
953 4203(76)90007-4.  
954  
955 Zappa, C. J., Raymond, P. A., Terray, E. A., and McGillis, W. R.: Variation in surface turbulence and the gas  
956 transfer velocity over a tidal cycle in a macro-tidal estuary. *Estuaries*, 26, 1401-1415, 2003. DOI:  
957 10.1007/BF02803649  
958  
959 Zhang, G. L., Zhang, J., Liu, S. M., Ren, J. L., and Zhao, Y. C.: Nitrous oxide in the Changjiang (Yangtze  
960 River) Estuary and its adjacent marine area: Riverine input, sediment release and atmospheric fluxes.  
961 *Biogeosciences* 7(11), 3505-3516, 2010. DOI: 10.5194/bg-7-3505-2010  
962